Chemical Physics 520 (2019) 108–121

Contents lists available at ScienceDirect

Chemical Physics

journal homepage: www.elsevier.com/locate/chemphys

Nonadiabatic conical nodes are near but not at an elliptical conical intersection

Peter W. Foster, David M. Jonas*

Department of Chemistry and Renewable and Sustainable Energy Institute, University of Colorado, Boulder, CO 80309, USA

ARTICLE INFO

Keywords:
Nonadiabatic eigenfunctions
Conical node
Conical intersection
Electronic index
Tangential node
Exact factorization

ABSTRACT

Numerical nonadiabatic eigenfunctions are calculated for 2D Jahn-Teller conical intersections with the elliptical shape found in square-symmetric molecules. Hunter's exact factorization is used to visualize the complete real-valued vibronic eigenfunctions. Point nodes are observed in the vibrational factor and the nodal structures are compared with those for circularly symmetric conical intersections. Without pseudo-rotation symmetry, essential *n*th order nodes at circular conical intersections split into *n* accidental conical nodes that are near but not at the elliptical conical intersection. For each eigenfunction, the integer electronic index that measures electronic state vector rotation around a closed vibrational path is locally stable to perturbations. Pairs of oppositely signed conical nodes can be generated or annihilated as Hamiltonian parameters are continuously varied. At annihilation, a tangential node with an electronic index of zero is created. For elliptical conical intersections, all eigenfunctions examined generate nonzero total vibrational probability density at the conical intersection.

1. Introduction

Nonadiabatic dynamics are important in many photochemical reactions and often proceed through conical intersections between adiabatic potential surfaces [1–10]. The adiabatic perspective faces interesting challenges when a conical intersection is submerged so that its energy lies below the zero point energy or is otherwise accessible. In these circumstances, the eigenfunctions can be delocalized over both adiabatic potential surfaces and their behavior at and around the conical intersection is of interest [11,12]. In spectroscopy, submerged conical intersections are readily accessible as an extreme limit of the dynamical Jahn-Teller effect [13–15] and can generate femtosecond nonadiabatic dynamics [10,16,17]. This paper is concerned with the eigenfunctions of low symmetry Jahn-Teller conical intersections, which occur in square-symmetric molecules such as porphyrins and phthalocyanines [18,19]. In such molecules, non-degenerate asymmetric vibrations lower the molecular symmetry to lift the electronic degeneracy between adiabatic potential energy surfaces.

For nonadiabatic systems, Hunter [20] developed an exact factorization [21,22] that closely parallels the Born-Oppenheimer factorization in many ways but also has fundamental differences. This factorization completely characterizes the exact eigenfunctions and is used to visualize nonadiabatic eigenfunctions here [23–25]. Each normalized eigenfunction is written as a product of a marginal vibrational factor and a conditional electronic factor. Like the Born-Oppenheimer factorization, each marginal vibrational factor is square-normalized for integration over all vibrational coordinates and, for every set of vibrational coordinates, each conditional electronic factor is square-normalized over the electronic coordinates. Unlike the Born-Oppenheimer factorization, the vibrational-coordinate dependent electronic factors vary from vibronic state to vibronic state and the vibrational factors are not orthogonal, which are both heavy prices. However, since the square of the vibrational factor gives the total vibrational probability density [24], Hunter's exact factorization is more natural for visualizing diffraction and imaging measurements [26,27] that probe the total vibrational probability density.

If only two electronic states are involved, the electronic factor, which depends on the vibrational coordinates, can be fully specified by one electronic angle. As a result, as shown in Refs. [23–25], a colored exact factorization with amplitude contours for the positive vibrational factor and color for the signed electronic factor provides complete visualization of real-valued nonadiabatic eigenfunctions with a single map [24]. This colored factorization led to the discovery of low dimensionality nodes in the exact factorization of nonadiabatic eigenfunctions [24] for an energy transfer Hamiltonian. These are in principle observable as isolated zeroes in the vibrational probability density. The dimensional considerations that govern the appearance of these nodes are similar to those for conical intersections between

* Corresponding author.
E-mail addresses: peter.foster@colorado.edu (P.W. Foster), david.jonas@colorado.edu (D.M. Jonas).

https://doi.org/10.1016/j.chemphys.2019.01.004

Available online 10 January 2019

adiabatic potential energy surfaces; for two electronic dimensions over two vibrational dimensions, one obtains point nodes. Since the surrounding vibrational amplitude has the shape of a right elliptical cone with the node at the vertex, these are called conical nodes [24]. These results do not contradict the idea that, with an infinite number of coupled electronic states, nonadiabatic couplings will always fill in nodes in the vibrational factor to some extent [22,28–30]. In practice, they suggest observable weakly avoided vibrational zeroes of low dimensionality in the total vibrational probability density [24].

Further exploration of a circularly symmetric Jahn-Teller Hamiltonian with a conical intersection that is submerged below the zero point level found that some eigenfunctions had vibrational amplitude at the conical intersection and some had essential nodes there [25]. These essential nodes are required by the circular symmetry when pseudo-rotation is excited and have integer orders given by the electronic index, which arises from variation of the electronic state vector around an encircling path [25]. For an essential node, the electronic index also gives the local radial dependence of the vibrational probability amplitude factor. With circular symmetry, essential first order nodes are circular conical nodes. Nonadiabatic wavefunction amplitude at a conical intersection is consistent with conjectures about nonzero amplitude at a conical intersection [11,12] and is critical for nonadiabatic tunneling [31–33].

Here we examine the relationship between conical intersections and nonadiabatic nodes for a lower symmetry Jahn-Teller Hamiltonian [15] which occurs for square-symmetric molecules. Square-symmetric molecules have either D_{4h} symmetry (the point group symmetry of a square) or C_{4v} symmetry (the point group symmetry of a square with different colors on the two faces). In molecules belonging to these point groups (and also molecules belonging to the D_4 and D_{2d} point groups isomorphic to C_{4v}), the Jahn-Teller effect is driven by non-degenerate vibrations of two different symmetries, giving the conical intersection an elliptical shape [34], but no tilt along its major or minor axes. All vibrational-electronic eigenfunctions remain doubly degenerate. Square-planar D_{4h} porphyrins have 4 non-planar distortions: doming, propellering, and saddling/ruffling [35]; these give distorted equilibrium geometries with C_{4v}, D_4, and D_{2d} point group symmetry, respectively. As a result, any single non-planar distortion does not alter the form of the linear Jahn-Teller coupling Hamiltonian. In a silicon naphthalocyanine molecule with D_{4h} molecular symmetry, a submerged conical intersection with Jahn-Teller stabilization energies of $\sim$1 meV drives electronic dynamics on $\sim$100 fs timescales [17,36,37].

In this paper, it will be shown that the lower symmetry around conical intersections in square-symmetric molecules has multiple consequences. Numerically exact calculations do not find nodes at the conical intersection. We found this numerical result surprising because the conical intersection has no tilt or asymmetry to drive nodes to one side over the other, so analytic perturbation theory is then used to demonstrate this result. A numerical example shows that first order nodes move continuously as the equilibrium Jahn-Teller displacement of the coupling coordinate is varied. Another numerical example shows that n^{th} order nodes, when not required by symmetry, split into n first order nodes that locally conserve the electronic index. Numerical examples in which the frequency of the coupling coordinate is varied exhibit node creation and annihilation phenomena. Numerically, these creation (annihilation) events generate (destroy) two nodes which have equal and opposite electronic indices. It is found numerically and shown analytically that node creation and annihilation proceeds through a nonadiabatic point node with a non-conical structure and an electronic index of zero; these are called tangential nodes. These node creation and annihilation phenomena also conserve the electronic index locally, so long as no node crosses the closed path along which the electronic index is calculated. To address the question of whether the electronic index has a globally conserved character, we report numerical results demonstrating that conical nodes can move in towards the conical intersection from large radius. These results, along with avoided crossings between eigenstates with different electronic indices around the perimeter examined here, suggest a globally conserved large radius electronic index either does not exist or is not easily accessible in numerical studies. To justify the title, it is shown that square-symmetric Jahn-Teller Hamiltonians can have global elliptical symmetry. Although the ellipticity in the shape of the adiabatic conical intersection can be transformed away, it is demonstrated that ellipticity cannot be transformed away from the nonadiabatic Hamiltonian. Ellipticity generates amplitude at an energetically accessible conical intersection for all eigenstates examined here. Finally, we discuss how probability amplitude at conical intersections might be experimentally observed.

2. Theory

This section begins with a brief presentation of the standard linear Jahn-Teller coupling Hamiltonian for square-symmetric point groups in a diabatic basis [18]. From there, globally valid vibrational coordinate dependent adiabatic potential energy surfaces and adiabatic electronic eigenstates with maximum continuity through the conical intersection are developed. A colored representation of the adiabatic electronic eigenstates clearly shows the phase discontinuity or cut radiating out from the conical intersection on each surface. Conical intersections have a sign which specifies the direction of electronic phase evolution for any path encircling the conical intersection [3]. This sign impacts the non-adiabatic eigenfunctions and is defined by a line integral following Ref. [25]. The doubly degenerate non-adiabatic eigenfunctions are uniquely chosen to be eigenstates of one reflection operator that follow a standard phase convention. This allows straightforward comparisons between eigenfunctions as Hamiltonian parameters are varied. After defining the colored exact factorization used for visualization of the complete nonadiabatic eigenfunctions, the integer electronic index developed in Ref. [25] to quantify the electronic state vector rotation [38] around a nonadiabatic node is defined and its key properties are briefly summarized.

2.1. The Jahn-Teller Hamiltonian

The Hamiltonian will be written down assuming the highest symmetry square-symmetric point group, D_{4h}, because symmetry species in the lower symmetry square-symmetric point groups can then be obtained through correlation tables [34]. Doubly degenerate electronic states subject to Jahn-Teller distortion have E_g or E_u symmetry at square-symmetric geometries. The $(n_x, n_y) = (2,1)$ and $(1,2)$ states for a particle in a 2D square box provide an example of an E_u symmetry electronic state. Diabatic electronic basis states x and y for the E state are assumed to be independent of the vibrational coordinates. Dimensionless normal coordinates and their canonically conjugate momenta can be obtained from internal vibrational coordinates [39] by a canonical scale transformation [40] of the normal coordinates that necessarily scales their generalized or conjugate momenta. Using the $\{|x\rangle, |y\rangle\}$ basis and dimensionless normal coordinates, the square-symmetric linear Jahn-Teller coupling Hamiltonian [18] (divided by $\hbar$) is

$$\hat{\boldsymbol{H}} = [(1/2)\omega_1(\hat{p}_1^2 + \hat{q}_1^2) + (1/2)\omega_2(\hat{p}_2^2 + \hat{q}_2^2)]\hat{\boldsymbol{I}} + \omega_1 d_1 \hat{q}_1[|x\rangle\langle x| - |y\rangle\langle y|] + \omega_2 d_2 \hat{q}_2[|x\rangle\langle y| + |y\rangle\langle x|] \quad (1)$$

where ω_i are the Jahn-Teller active vibrational frequencies (i = 1 or 2), $\hat{q}_i$ and $\hat{p}_i$ are the dimensionless normal coordinate position and momentum operators, d_i are the equilibrium Jahn-Teller displacements for those vibrations in dimensionless normal coordinates, and $\hat{\boldsymbol{I}} = |x\rangle\langle x| + |y\rangle\langle y|$ is the electronic identity operator for the Jahn-Teller degenerate states. The first line is a harmonic oscillator Hamiltonian for two vibrations. The second and third lines contain linear vibrational-electronic couplings, which are specified by the equilibrium Jahn-Teller displacements of the lower adiabatic potential energy surface. All vibrations without a linear Jahn-Teller coupling have been omitted. In

this paper, all vibrational frequencies and energy eigenvalues will be given in wavenumbers (which must be multiplied by $2\pi c$ to convert into angular frequencies).

In the D_{4h} point group, the Jahn-Teller active asymmetric vibrations q_1 and q_2 have b_{1g} and b_{2g} symmetry, respectively (correlating to b_1 and b_2, respectively, in the 3 isomorphic lower symmetry groups). Using the terminology for more general conical intersections [41], q_1 is the tuning coordinate (g) and q_2 is the coupling coordinate (h). For a particle in a square 2D box, rectangular and diamond symmetry lowering deformations of the square box would have b_{1g} and b_{2g} symmetry [37,42–44]. There are equal numbers of b_{1g} and b_{2g} vibrations in any D_{4h} symmetry molecule, but these Jahn-Teller active vibrations are non-degenerate (unlike other n-fold point group symmetries with Jahn-Teller distortions) [34]. Low frequency vibrations sometimes occur in b_{1g}/b_{2g} pairs with similar frequencies and Jahn-Teller displacements [45]. With equal frequencies ($\omega_1 = \omega_2$) and displacements ($d_1 = d_2$), this Hamiltonian generates [18] a circularly symmetric conical intersection [13,46].

2.2. Adiabatic surfaces

The adiabatic electronic Hamiltonian is obtained by neglecting the kinetic energy operators and regarding the vibrational coordinates as parameters:

$$\hat{\boldsymbol{H}}_{elec}(q_1, q_2) = [(1/2)\omega_1 q_1^2 + (1/2)\omega_2 q_2^2]\hat{\boldsymbol{I}} + \omega_1 d_1 q_1 [|x\rangle\langle x| - |y\rangle\langle y|] + \omega_2 d_2 q_2 [|x\rangle\langle y| + |y\rangle\langle x|]. \quad (2)$$

The adiabatic potential energy surfaces are obtained by diagonalizing the electronic Hamiltonian at each coordinate (q_1, q_2):

$$\hat{\boldsymbol{H}}_{elec}(q_1, q_2)|\pm;q_1, q_2\rangle = U_{\pm}(q_1, q_2)|\pm;q_1, q_2\rangle \quad (3)$$

The adiabatic potential surfaces are the electronic energy eigenvalues [47],

$$U_{\pm}(q_1, q_2) = [(1/2)\omega_1 q_1^2 + (1/2)\omega_2 q_2^2] \pm \sqrt{(\omega_1 d_1 q_1)^2 + (\omega_2 d_2 q_2)^2}. \quad (4)$$

As shown in Fig. 1, the two surfaces intersect at the origin (the square-symmetric geometry) and together form a right elliptical double cone in its immediate neighborhood. Along the q_1-axis ($q_2 = 0$), slices through the pair of potential surfaces give parabolas with positive curvature that intersect at the origin and have their minima displaced to $q_1 = \pm d_1$, the equilibrium Jahn-Teller displacement parameter used here to specify the linear vibrational-electronic coupling. Both minima are lower than the conical intersection by the Jahn-Teller stabilization energy $(D\omega)_1 = (1/2)\omega_1 d_1^2$. Similar statements hold for the slice along the q_2-axis. In 2D, the minima for slices along the coordinate axis with the smaller stabilization energy become saddle points separating true minima along the coordinate axis with the larger stabilization energy. The lower surface has two symmetry related minima separated by two symmetry related saddle points and a local maximum that touches the bottom of the upper cone at its minimum [18,34]. The point of contact between upper cone and lower surface is the conical intersection, and the two surfaces locally form a right elliptical double cone around it. The conical intersection is located at the coordinate origin and the zero of energy. Moving from one adiabatic surface onto the other on passing through the conical intersection makes the pair of potential energy surfaces have continuous derivatives with respect to vibrational coordinates. For this reason, Longuet-Higgins et al. referred to the two adiabatic electronic eigenvalue surfaces as continuations of each other [13].

The real-valued adiabatic electronic energy eigenstates depend only on the adiabatic mixing angle

$$\phi(q_1, q_2) = \text{atan2}\ (\omega_2 d_2 q_2,\ \omega_1 d_1 q_1) \quad (5)$$

where atan2(y, x) extends arctangent(y/x) over a 2π range. Square-symmetry dictates the adiabatic electronic character up to a sign on the $q_1 = 0$ and $q_2 = 0$ lines, but does not dictate the quantitative electronic variation with angle in the (q_1, q_2) plane, which depends on the coupling parameters through Eq. (5). [In contrast, for circularly symmetric conical intersections, which have $\omega_1 d_1 = \omega_2 d_2$, the adiabatic mixing angle ϕ becomes equal to the polar coordinate in the (q_1, q_2) plane.] For real-valued eigenfunctions, Longuet-Higgins showed the adiabatic electronic eigenfunctions must encounter a sign change discontinuity for any closed curve encircling the conical intersection [48]. This sign change discontinuity or cut radiates out from the conical intersection point, but its location is arbitrary [49]. The adiabatic electronic eigenstates are chosen for maximum continuity as:

$$|-;\phi\rangle = \text{ssqw}(\phi/2)\{\sin(\phi/2)|x\rangle - \cos(\phi/2)|y\rangle\} \quad (6a)$$

for the lower adiabatic state and

$$|+;\phi\rangle = \text{csqw}(\phi/2)\{\cos(\phi/2)|x\rangle + \sin(\phi/2)|y\rangle\} \quad (6b)$$

for the upper adiabatic state. Eqs. (6a) and (6b) have been simplified by defining a sinusoidal square wave function

$$\text{ssqw}(\vartheta) = \text{signum}[\sin(\vartheta)] \quad (7a)$$

and a cosinusoidal square wave function

$$\text{csqw}(\vartheta) = \text{signum}[\cos(\vartheta)] \quad (7b)$$

by means of the standard [50] signum function

$$\text{signum}(\xi) = \begin{cases} +1 & (\xi > 0) \\ 0 & (\xi = 0) \\ -1 & (\xi < 0) \end{cases} \quad (8)$$

With this form of Eqs. (6a) and (6b), the adiabatic mixing angle ϕ can take on any real value. The trigonometric square wave functions specify the locations of cuts (see Fig. 1). Here, the cuts on the two surfaces have been arranged into a maximally continuous single cut along $q_2 = 0$ such that the lower surface cut for $q_2 < 0$ connects to the upper surface cut for $q_2 > 0$ and separates $\pm\,|y\rangle$ on both surfaces. Eqs. (6a) and (6b) show that $|+;\phi + \pi\rangle = |-;\phi\rangle$ everywhere except at the conical intersection point, where both are undefined. As can be seen from the surface colors in Fig. 1, moving from one adiabatic surface to the other on passing through the conical intersection makes the pair of adiabatic electronic eigenstates continuous across the conical intersection (except for the undefined electronic character of the separate surfaces at the conical intersection point). For this reason, Longuet-Higgins et al. also referred to the two adiabatic electronic eigenstates as continuations of each other [13].

2.3. The sign of the conical intersection

Conical intersections have a sign [3] which can be defined by the sign of any counterclockwise line integral around the conical intersection [25]:

$$\gamma(C) = \frac{1}{2\pi}\int_C d\Theta^a(q_1, q_2). \quad (9)$$

where $\Theta^a_{\pm}(q_1, q_2) \equiv \arctan[\langle y|\pm;\phi\rangle/\langle x|\pm;\phi\rangle]$ are diabatic to adiabatic transformation angles. From Eqs. (6a) and (6b), the transformation angles are $\Theta^a_{-}(q_1, q_2) = (\phi - \pi)/2$ over the domain $\phi = (0, 2\pi)$ and $\Theta^a_{+}(q_1, q_2) = \phi/2$ over the domain $\phi = (-\pi, \pi)$; each becomes undefined at its cut. The line integral starts and stops at the cut for the single-valued Θ^a used here. For real-valued electronic states, the phase angle is an integer multiple of π and gives the adiabatic electronic sign discontinuity found by Longuet-Higgins [13,48,51,52] for closed paths around a conical intersection (an example of a geometric phase [53]). The sign of a conical intersection, signum(γ), depends on the phase convention for the diabatic electronic basis set but not on arbitrary adiabatic eigenfunction sign or phase. Any line integral around the conical intersection is $\gamma(C) = +1/2$ for *either* surface in Fig. 1, so the sign of this conical intersection is positive.

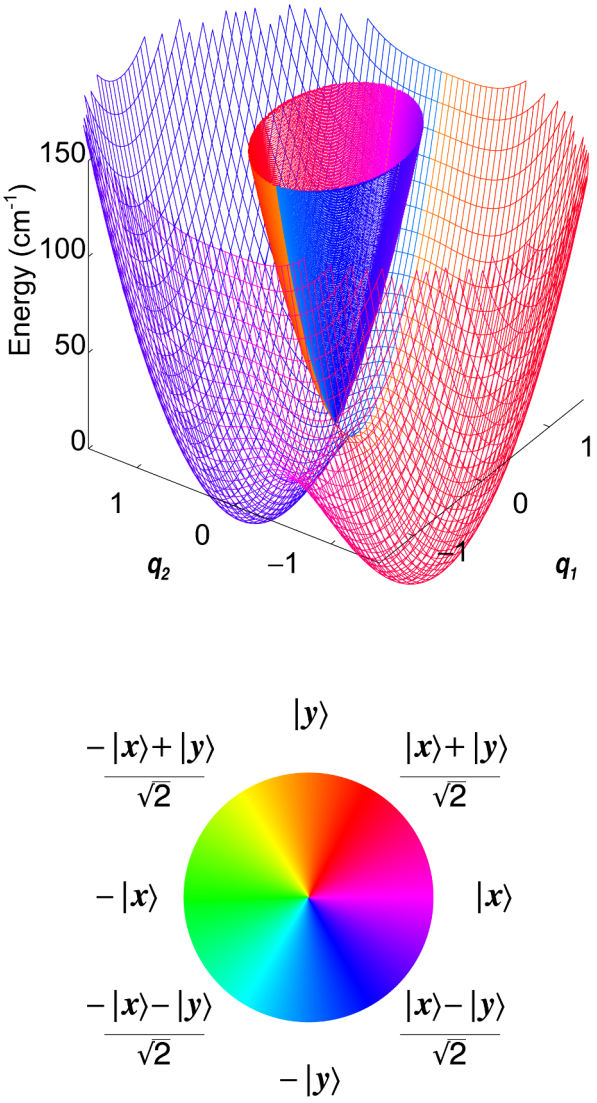

Fig. 1. Potential Surfaces around the Conical Intersection for a Square-Symmetric Molecule. Top) The adiabatic potential energy surfaces for a doubly degenerate E symmetry electronic state as a function of Jahn-Teller active normal coordinates (q_1, q_2) with b_{1g} and b_{2g} symmetry. The Hamiltonian parameters in Eq. (1) have accidentally equal vibrational frequencies $\omega_1 = \omega_2 = 200\,\mathrm{cm}^{-1}$ with unequal displacements $d_1 = 0.4$ and $d_2 = 0.8$ along q_1 and q_2, respectively. The lower surface has minima [front right and back left] at $(0, \pm d_2)$ that are stabilized by $(D\omega)_2 = 64\,\mathrm{cm}^{-1}$ below the conical intersection. The two saddle points [front left and back right] at $(\pm d_1, 0)$ are stabilized by $(D\omega)_1 = 16\,\mathrm{cm}^{-1}$. The upper cone has roughly elliptical cross sections with major axes along q_1. The color of each potential surface at each coordinate indicates the adiabatic electronic eigenfunction according to the color wheel. Bottom) Color wheel used to indicate electronic eigenfunctions for the adiabatic potential surfaces above and for nonadiabatic eigenfunctions throughout the rest of the paper. The 2π angular range is divided into 64 discrete colors. The adiabatic potential surfaces show continuous coloring through the conical intersection and an eigenfunction sign-change discontinuity or cut (arbitrarily located along $q_2 = 0$) that is required by the geometric phase.

2.4. Exact nonadiabatic eigenstates

The nonadiabatic eigenfunctions solve the full time-independent Schrodinger equation

$$\hat{\boldsymbol{H}}\psi_m(\boldsymbol{r}, q_1, q_2) = E_m\psi_m(\boldsymbol{r}, q_1, q_2) \tag{10}$$

and depend on both electronic (**r**) and vibrational coordinates. Although the degeneracy of the adiabatic potential energy surfaces is lifted everywhere but at the conical intersection, the nonadiabatic vibrational-electronic eigenstates of the square-symmetric Jahn-Teller Hamiltonian all remain doubly degenerate. The degeneracy arises because the total Hamiltonian in Eq. (1) has a molecular symmetry group [54] that remains isomorphic to the square-symmetric point group even when Jahn-Teller distortions lower the equilibrium point group symmetry [18]. The square-symmetric Hamiltonian separately commutes with two mutually non-commuting reflection operators σ_v and σ_d; this requires degeneracy [55] and imposes symmetries on the eigenstates beyond those required by four-fold rotational symmetry. Under these reflection operators, the asymmetric coordinates and diabatic electronic basis states transform as [37]:

$$\sigma_v q_1 = +q_1, \quad \sigma_v q_2 = -q_2, \tag{11a}$$

$$\sigma_v\ |x\rangle = +|x\rangle, \quad \sigma_v\ |y\rangle = -|y\rangle \tag{11b}$$

and

$$\sigma_d q_1 = -q_1, \quad \sigma_d q_2 = +q_2, \tag{11c}$$

$$\sigma_d\ |x\rangle = +|y\rangle, \quad \sigma_d\ |y\rangle = +|x\rangle \tag{11d}$$

Pairs of doubly degenerate eigenstates can be chosen as simultaneous eigenstates of the Hamiltonian and either reflection operator.

When the conical intersection parameters generate circular symmetry, the eigenfunctions have an additional rigorous pseudo-rotation quantum number j and an approximate vibrational quantum number v. Vibrational quantum numbers characterize such eigenfunctions well in the limits of small d (circular 2D harmonic oscillator quantum numbers) and large d (separable adiabatic radial vibration on the lower surface) [13,56]. Circular 2D harmonic oscillator quantum numbers are used here to describe elliptical conical intersection eigenstates by correlation to eigenstates of a circular conical intersection with reasonably small Jahn-Teller displacement d. These quantum numbers are not "good" for elliptical conical intersections, just convenient correlation labels that provide an energetic point of reference.

2.5. Colored exact factorization

To simultaneously visualize a complete nonadiabatic eigenfunction, we use Hunter's exact factorization [20,29]. Each normalized eigenfunction $\psi_m(\boldsymbol{r}, q_1, q_2)$ is written as a product of an everywhere positive marginal vibrational amplitude factor,

$$Þ_m(q_1, q_2) = \sqrt{\int \psi_m^*(\boldsymbol{r}, q_1, q_2)\psi_m(\boldsymbol{r}, q_1, q_2)\mathrm{d}\boldsymbol{r}} \tag{12}$$

and a signed conditional electronic factor

$$\mathrm{K}_m(\mathbf{r}; q_1, q_2) = \psi_m(\mathbf{r}, q_1, q_2)/Þ_m(q_1, q_2) \tag{13}$$

Like Born-Oppenheimer factors, each exact vibrational factor is square-normalized over the vibrational coordinate space and each conditional electronic factor is square-normalized over the electronic space (**r**) at each vibrational coordinate (q_1, q_2). The conditional electronic factor is a unit vector in the electronic state space. If the vibrational amplitude factor has a node, the exact factors are not separately acceptable wavefunctions, motivating the use of the Icelandic letter thorn, Þ, to emphasize that the vibrational factor is the square root of the diagonal element of the reduced vibrational density operator obtained by tracing over electronic states. The exact vibrational factor for a real-valued nonadiabatic eigenfunction may have integer-order essential nodes if they are required by symmetry and accidental first order conical nodes, which become likely when the vibrational dimensionality exceeds the electronic dimensionality. When only two electronic states (x and y) are involved, the exact electronic factor at each set of vibrational coordinates can be fully specified (in character and phase) for each nonadiabatic state m by the electronic angle

$$\Theta_m(q_1, q_2) \equiv \mathrm{atan2}(\langle y\,|\psi_m\rangle, \langle x\,|\psi_m\rangle) = \mathrm{atan2}(\langle y\,|\mathrm{K}_m\rangle, \langle x\,|\mathrm{K}_m\rangle), \tag{14}$$

which becomes undefined if the vibrational amplitude factor is zero. Representing the positive vibrational factor by amplitude contours and the signed electronic factor by color (referencing the color wheel in Fig. 1) allows a single map to completely specify a real-valued nonadiabatic eigenfunction [24]. A price paid for using this colored exact factorization is that visualization of linear combination states requires thinking about how the mixing of colors represents the addition of vibrational amplitude weighted electronic factors.

2.6. The electronic index

A key property of the nonadiabatic eigenfunctions is the electronic index $\eta(C)$ for line integrals around any simple closed counterclockwise path C in the vibrational coordinate space that does not pass through a node [25],

$$\eta(C) = \frac{1}{2\pi} \oint_C d\Theta_m(q_1, q_2) \tag{15}$$

Visually, the electronic index equals the integer number of net counterclockwise turns around the color wheel on the path C. Like the sign of a conical intersection, the electronic index depends on the phase convention for the diabatic electronic basis states $|x\rangle$ and $|y\rangle$, but is independent of the arbitrary overall sign of the eigenfunction. As a result, electronic indices for different eigenstates are significant relative to each other. For a two-dimensional electronic state space over a two dimensional vibrational space, Ref. [25] proved that the integer electronic index depends only on the number, order, and sign of the nonadiabatic nodes enclosed by the path.

3. Calculations

The diabatic basis set Hamiltonian diagonalization computations are similar to those in Ref. [25]. For high spatial resolution, harmonic oscillator basis state coefficients are found and used to construct the nonadiabatic eigenfunctions of Eq. (10). All harmonic oscillator basis states are centered at the origin. Harmonic oscillator matrix elements are obtained analytically [36,39]. Calculations use a truncated vibronic Hamiltonian matrix that includes all vibrational states with $v_1 + v_2 \leqslant N$ (roughly, this includes all 2D harmonic oscillator basis states up to a certain energy, which provides faster convergence compared to the separate maxima for v_1 and v_2 used in Ref. [25]). The number of vibrational basis states on each diabatic electronic state is $(N + 1)(N + 2)/2$, so each calculation includes a total of $(N + 1)(N + 2)$ diabatic vibronic basis states. The Hamiltonian is diagonalized using the DEVCSF routine from the IMSL library which uses an implicit QR algorithm [57] to evaluate eigenvalues and eigenvectors. All results shown are for $N = 39$. In addition to the convergence checks in Ref. [25], the eigenvalues were checked for accuracy against Judd's exact results [58], which provide some analytic eigenvalues for specific circular symmetry conical intersection parameters (see Table S1 and Fig. S1 in Supplementary Material). This check indicates 14-digit numerical accuracy for the eigenvalues. Supplementary Table S2 and Fig. S2 show eigenvalues for a square-symmetric Hamiltonian.

A numerically stable basis set rotation is applied to each pair of degenerate eigenstates to find states with σ_d symmetry [37]. The basis set is then rotated by $\pi/4$ to find states with σ_v symmetry. These states are then separated into states with eigenvalues of + 1 and − 1 with respect to the σ_v operator. Then the vibrational amplitude and electronic factor are calculated using Eqs. (12) and (13), respectively. Finally, overall eigenfunctions signs are chosen to match perturbation theory results for small d_2. All of the nonadiabatic eigenfunctions shown in the main body of this paper have a σ_v eigenvalue of +1 so that $\sigma_v\ |\psi_m\rangle = +|\psi_m\rangle$. Pairs of degenerate eigenstates of σ_v and the alternative representation of each pair as eigenstates of σ_d are shown together in Supplemental Material Fig. S3.

4. Results

4.1. Effects of unequal linear Jahn-Teller couplings

Fig. 2 shows the colored exact factorization of the lowest eigenstates for several Jahn-Teller Hamiltonians with different equilibrium displacements for the coupling coordinate. (Fig. S2 shows that the energy eigenvalues undergo avoided crossings [59] as a function of the linear Jahn-Teller coupling parameter d_2.) In the rightmost column of Fig. 2, both Jahn-Teller displacements are $d_1 = d_2 = 0.4$, generating a circularly symmetric conical intersection. This circularly-symmetric case is not general, and differences between d_1 and d_2 are expected for square-symmetric molecules. The eigenstates in the rightmost column are similar to those in column 1 of Fig. 2 from Ref. [25] where $d_1 = d_2 = 0.316$. However, some arbitrary overall eigenfunction signs are different here in order to more simply connect with results from perturbation theory starting from Hougen's accidental Born-Oppenheimer [18] case. For $d_2 = 0$, the phases have been chosen to agree with the phase convention of Papousek and Aliev [39] as in Ref. [25].

In all five columns of Fig. 2, every $\sigma_v = +1$ eigenstate shown is degenerate with an eigenstate having $\sigma_v = -1$ and any linear combination of the degenerate eigenstates is also an energy eigenstate. Linear combinations of the doubly degenerate eigenstates with $\sigma_v = \pm 1$, $\sigma_d = \pm 1$, and signed pseudo-rotation quantum numbers $\pm j$ are shown for a circularly symmetric conical intersection in Fig. 2 from Ref. [25] and the transformations between them are discussed there. Fig. S3 shows the set of $\sigma_v = \pm 1$ and $\sigma_d = \pm 1$ eigenfunctions for the elliptical conical intersection in the fourth column of Fig. 2.

Important differences between the states studied here and those studied in Ref. [25] arise because circular symmetry generates a conserved pseudo-rotation quantum number j. In Fig. 2, some circular symmetry eigenstates have higher order essential nodes that do not occur without pseudo-rotation symmetry. Essential nodes occur because j takes on half-odd integral values $(-v - 1/2, \ldots -3/2, -1/2, +1/2, +3/2, \ldots v + 1/2)$ and requires radial amplitude power law exponents of at least $\mathrm{P}_{v,j}(\rho, \phi) \propto \rho^{|j|-(1/2)}$ in the vibrational amplitude [25]. Further, these essential nodes have an electronic index with a magnitude of exactly $|j| - (1/2)$ for simple closed counterclockwise paths that encircle the essential node but do not encircle any other node. This index is negative (clockwise around the color wheel for a counterclockwise path) for all three essential nodes in the rightmost column of Fig. 2 and positive (counter-clockwise around the color wheel for a counterclockwise path) for the three essential nodes in the leftmost column of Fig. 2. This change in sign of the index is accompanied by a change in sign of the conical intersection. The leftmost column in Fig. 2 here differs from Fig. 6 of Ref. [25] in reversing the sign of the conical intersection by changing the sign of d_2 instead of d_1. Examination of the Hamiltonian in Eq. (1) shows that changing the sign of the equilibrium Jahn-Teller displacement d_i is equivalent to changing the sign of the coordinate q_i. While both the electronic index of a node and the sign of a conical intersection depend on the phase convention for the electronic basis states, their physically meaningful ratio does not. As proven in Ref. [25], the electronic index for a simple closed path that encircles several nodes is the sum of the electronic indices for the enclosed nodes. Such summed electronic indices are stable with respect to the symmetry lowering perturbations in the second and fourth columns of Fig. 2. However, as the displacement d_2 is varied over a wider domain from 0 to 1 for this family of square-symmetric Jahn-Teller Hamiltonians (in which all other parameters remain fixed), Fig. S2 shows avoided crossings between states with different summed electronic indices; these avoided crossings indicate that the summed electronic indices are not globally conserved over the vibrational coordinate region shown in Fig. 2.

The changes in coupling coordinate displacement from left to right in Fig. 2 lower the symmetry of and then annihilate a negative conical intersection at an accidental adiabatic point before creating a positive

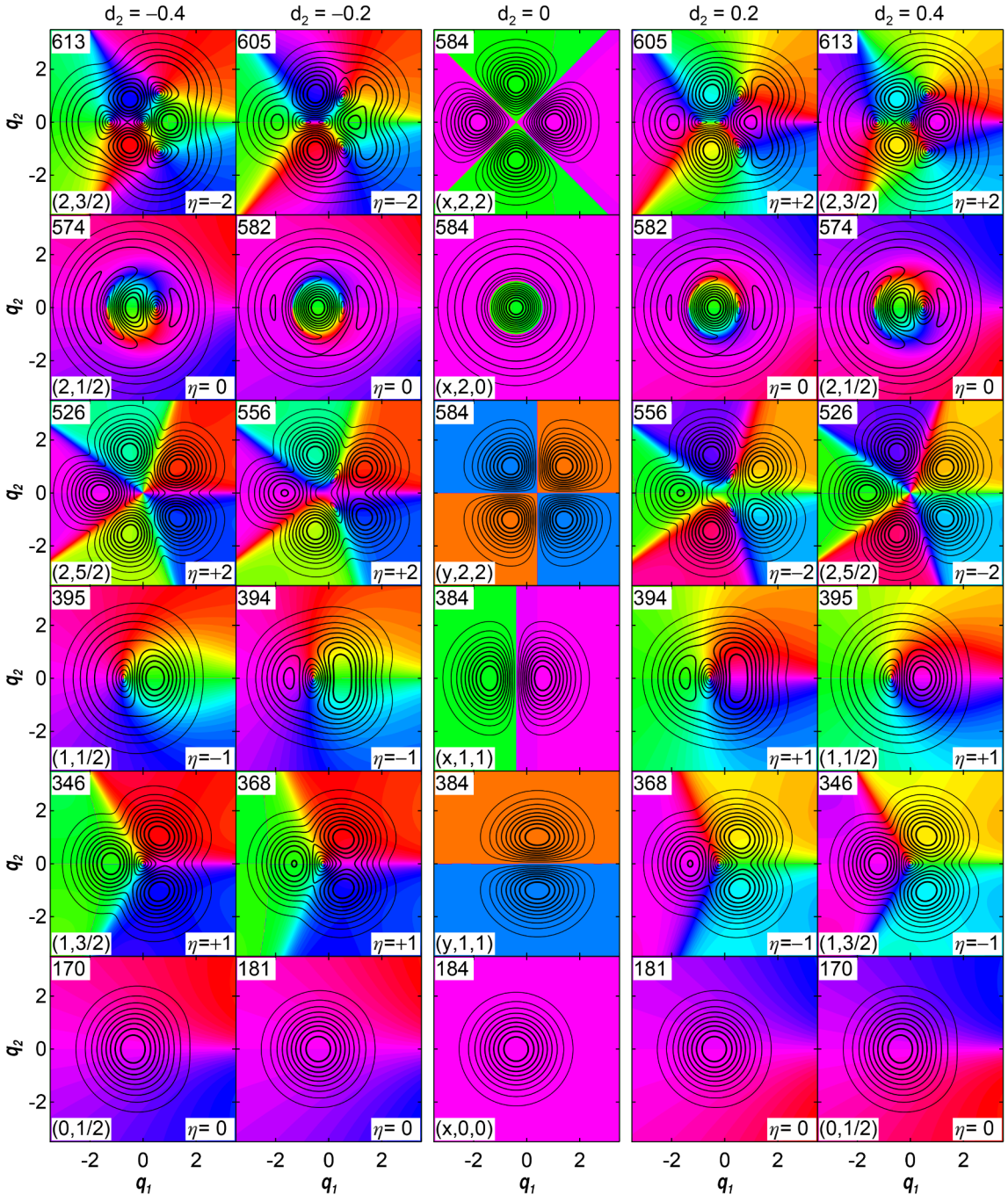

Fig. 2. Effects of varying Jahn-Teller displacement for the coupling coordinate. The five columns each have six panels showing the probability amplitude and electronic character of the six lowest energy eigenstates with $\sigma_v = +1$ for the Jahn-Teller Hamiltonian with vibrational frequencies $\omega_1 = \omega_2 = 200\ cm^{-1}$ and Jahn-Teller displacement $d_1 = 0.4$ for the tuning coordinate. The five columns systematically vary the Jahn-Teller displacements d_2 for the coupling coordinate. In each panel, the contour interval is 10% of the maximum probability amplitude for that state, with thicker contour lines for higher amplitude. The color wheel in Fig. 1 is used to represent electronic character. In each column, the lowest energy state is on the bottom and energy increases upward. In each panel, the label at upper left gives the eigenstate energy in wavenumbers and the label at lower right specifies the electronic index η for paths around the perimeter. The leftmost and rightmost columns have circular symmetry conical intersections with opposite signs. These eigenstates have a good vibrational quantum number v and a rigorous absolute value of the half-odd integral pseudo-rotation quantum number $|j|$ given at lower left $(v, |j|)$. In each column, three eigenfunctions have essential nodes of order $(|j| - 1/2)$ at the conical intersection (346, 526, and 613), and three have accidental conical nodes elsewhere (395, 574, and 613). The second and fourth columns have non-adiabatic Hamiltonians with elliptical conical intersections, which break pseudo-rotation symmetry. The eigenstates do not have rigorous quantum numbers beyond σ_v and have only accidental conical nodes. None of the accidental nodes occur at the conical intersection at the origin. The middle column is an accidental Born-Oppenheimer case with adiabatic nodal lines or curves indicated by abrupt color changes. In the middle column, degenerate states are chosen so each has a definite adiabatic electronic state (x or y), vibrational quantum number v, and absolute value of the vibrational angular momentum $|\ell|$ about the equilibrium geometry on its adiabatic potential surface given at lower left $(x/y, v, |\ell|)$.

conical intersection and restoring circular symmetry. Two level crossings occur as the conical intersection is annihilated: eigenstates correlating to ($v = 1$, $|j| = 3/2$) and ($v = 1$, $|j| = 1/2$) on the left cross at $d_2 = 0$ to correlate with ($v = 1$, $|j| = 1/2$) and ($v = 1$, $|j| = 3/2$), respectively, on the right; similarly, ($v = 2$, $|j| = 5/2$) and ($v = 2$, $|j| = 3/2$) on the left cross to become ($v = 2$, $|j| = 3/2$) and ($v = 2$, $|j| = 5/2$), respectively, on the right; ($v = 2$, $|j| = 1/2$) passes through this higher energy level crossing. (The level crossings at $d_2 = 0$ are examined closely in Fig. S4 of the Supplementary Material.) For each eigenstate, the electronic index for paths around the perimeter is conserved through these crossings over the range of equilibrium Jahn-Teller displacements shown in Fig. 2.

4.2. Nodes near, but not at, conical intersections

In square-symmetric molecules, Hamiltonians with circular symmetry and their eigenstates with essential nodes are improbable (zero probability) because they require two exact equalities between continuously variable parameters. Similarly, the adiabatic case with nodal lines and curves in the middle column is improbable (zero probability) because it requires that one parameter be exactly zero. The eigenfunctions shown in the second and fourth columns of Fig. 2 also require a one parameter equality (equal frequencies) for square-symmetric molecules. For these nonadiabatic eigenfunctions, the only nodes are accidental conical nodes, each with an elliptical shape. So long as no node crosses the enclosing path as the Hamiltonian symmetry is lowered, the electronic index for the square-symmetric case is equal to the electronic index for the circularly symmetric case. For 5 of the 6 states in Fig. 2, conical nodes simply change their position continuously as a function of coupling coordinate displacement until they disappear along with the conical intersection at $d_2 = 0$. For the 6th state ($v = 2$, $|j| = 5/2$), the essential second order node splits into two first order conical nodes with the same sign as the symmetry is lowered. This splitting preserves the total electronic index for small radius paths that enclose the origin and both split nodes.

Conical nodes need not occur at the conical intersection for elliptical conical intersections in square-symmetric molecules. Close inspection of columns 2 and 4 in Fig. 2 indicates that conical nodes occur near the conical intersection, but not at the conical intersection. This result can be understood based on the nonadiabatic eigenstates shown in Fig. 3, which can be accurately obtained from first order degenerate perturbation theory starting from a basis of eigenstates for $d_2 = 0$.

In square-symmetric molecules, the equilibrium Jahn-Teller displacements along any pair of Jahn-Teller active modes are independent of each other. When either displacement d_i is zero, the Jahn-Teller Hamiltonian accidentally becomes an adiabatic Hamiltonian with analytic solutions [18]. The adiabatic electronic eigenstates become $|x\rangle$ and $|y\rangle$, which are allowed to cross because they have different symmetries. The vibrational coordinates q_1 and q_2 become separable, with harmonic oscillator quantum numbers v_1 and v_2 (this basis is useful even when the vibrational frequencies are different). Superscripts on the vibrational quantum numbers will indicate which adiabatic electronic basis state they are vibrational eigenstates of (*i.e.* their displacements for the unperturbed Hamiltonian with $d_2 = 0$). With $d_2 = \delta$, the degenerate adiabatic basis states $|x\rangle|v_1^x = 1\rangle|v_2^x = 0\rangle$ and $|y\rangle|v_1^y = 0\rangle|v_2^y = 1\rangle$ both have $\sigma_v = +1$ and are directly coupled by the off-diagonal tuning coordinate perturbation operator

$$\hat{H}_1 = \omega_2 \delta \hat{q}_2 [\,|x\rangle\langle y| + |y\rangle\langle x|\,] \tag{16}$$

The direct matrix element coupling these two states is given by

$$\begin{aligned} H_{y01,x10} &= \langle v_2^y = 1|\langle v_1^y = 0|\langle y|\ \hat{H}_1\ |x\rangle|v_1^x = 1\rangle|v_2^x = 0\rangle \\ &= \omega_2 \delta \langle v_1^y = 0|\ v_1^x = 1\rangle\langle v_2^y = 1|\ q_2\ |v_2^x = 0\rangle \\ &= \omega_2 \delta\ \ [\sqrt{2}\, d_1 exp(-d_1^2)][1/\sqrt{2}] \end{aligned} \tag{17}$$

On the last line, the first factor in brackets is the Franck-Condon overlap integral for mode 1 (relative to each other, the electronic states x and y are displaced by $2d_1$), and the second factor in brackets is the harmonic oscillator matrix element for mode 2. For the parameters used in Fig. 3, $H_{y01,x10} \approx 6.817 \times 10^{-9}\,\mathrm{cm}^{-1}$. Degenerate first-order perturbation theory [55] yields the eigenstates

$$|\psi_+\rangle = (1/\sqrt{2})[\,|y\rangle|v_1^y = 0\rangle|v_2^y = 1\rangle + |x\rangle|v_1^x = 1\rangle|v_2^x = 0\rangle\,] \tag{18}$$

And

$$|\psi_-\rangle = (1/\sqrt{2})[\,|y\rangle|v_1^y = 0\rangle|v_2^y = 1\rangle - |x\rangle|v_1^x = 1\rangle|v_2^x = 0\rangle\,] \tag{19}$$

with eigenvalues

$$E_\pm^{(1)} = E^{(0)} \pm H_{y01,x10} \tag{20}$$

where $E^{(0)} = H_{y01,y01} = H_{x10,x10} = 384\,\mathrm{cm}^{-1}$. Since δ is positive, the lower eigenstate is the antisymmetric linear combination and the upper eigenstate is the symmetric linear combination. For this pair of states, all other couplings are of second order. Since the contributing adiabatic basis states have nodal lines that cross, their crossing point locates the conical node at ($q_1 = -d_1$, $q_2 = 0$).

A slightly more complicated analysis can be performed for states

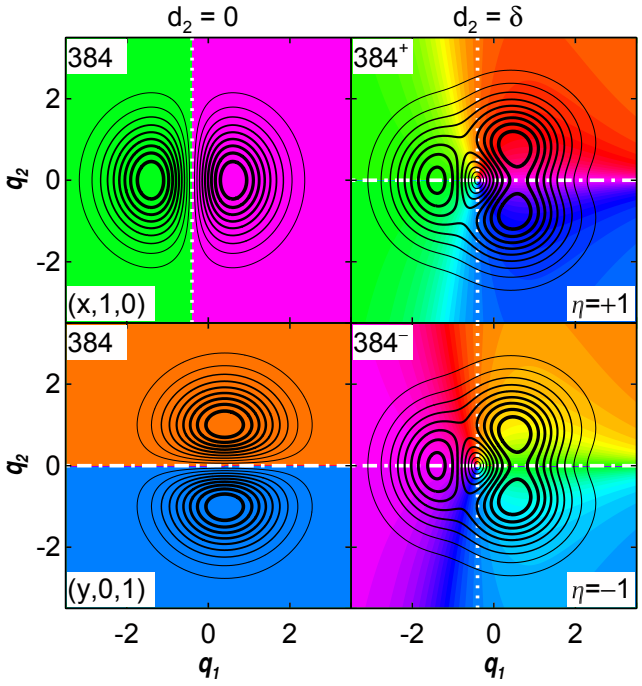

Fig. 3. Accidental Conical Nodes are near but not at the Conical Intersection. Left Column) Probability amplitude and electronic character for eigenfunctions with $\sigma_v = +1$ and one quantum of vibration for an accidental Born-Oppenheimer Hamiltonian with parameters $\omega_1 = \omega_2 = 200\,\mathrm{cm}^{-1}$, $d_1 = 0.4$, and $d_2 = 0$. Contour intervals are 10% of each state's maximum probability amplitude, and are thicker for higher amplitude. The top eigenfunction has quantum numbers (x, $v_1 = 1$, $v_2 = 0$) and has a vertical nodal line (dotted white) through the equilibrium geometry of adiabatic electronic state x, ($q_1 = -d_1$, $q_2 = 0$). The bottom eigenfunction has quantum numbers (y, $v_1 = 0$, $v_2 = 1$) and has a horizontal nodal line (dot-dashed white) through the equilibrium geometry of adiabatic electronic state y, ($q_1 = +d_1$, $q_2 = 0$). Both energy eigenvalues are exactly $384\,\mathrm{cm}^{-1}$. Right Column) Probability amplitude and electronic character for eigenfunctions with $\sigma_v = +1$ and one quantum of vibration for a nonadiabatic Hamiltonian with parameters $\omega_1 = \omega_2 = 200\,\mathrm{cm}^{-1}$, $d_1 = 0.4$, and $d_2 = \delta$, where $\delta = 10^{-10}$. The nonadiabatic energy eigenvalues are non-degenerate, with shifts of $\pm\, 6.818 \times 10^{-9}\,\mathrm{cm}^{-1}$ to 384^+ (top) and 384^- (bottom). For both nonadiabatic eigenfunctions, the dot-dashed and dashed nodal lines of the projections onto adiabatic basis states intersect at the conical node, which occurs at ($q_1 = -d_1$, $q_2 = 0$) in the limit as δ tends to zero.

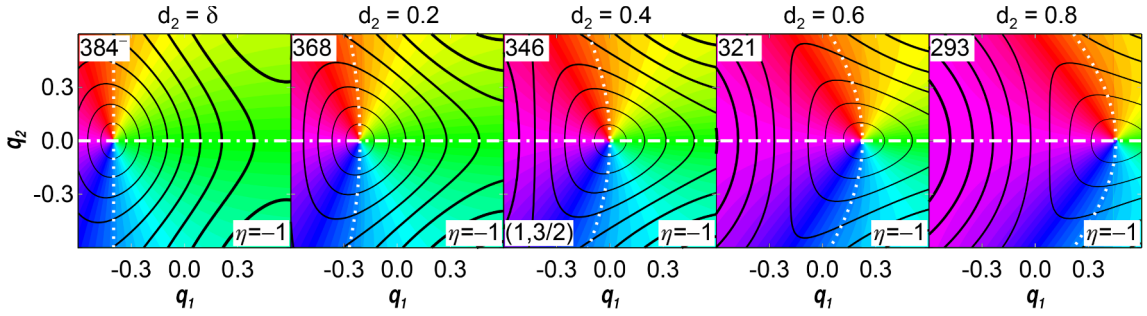

Fig. 4. Varying the coupling coordinate displacement. The five panels show how variation of d_2 affects the conical node in the second lowest energy $\sigma_v = +1$ eigenstate of the Jahn-Teller Hamiltonian with vibrational frequencies $\omega_1 = \omega_2 = 200\ cm^{-1}$ and $d_1 = 0.4$. Panels are labeled at upper left by the eigenstate energy in cm^{-1}. Each panel overlays the nodal curves in the eigenfunction projections onto adiabatic electronic states x (dotted white curve) and y (dot-dashed white line). Contour intervals are 10% of maximum amplitude. From left to right: $d_2 = \delta$) here $\delta = 10^{-10}$ and the conical node is located at $q_1 = -d_1 = -0.4$. This is a close-up of the lower right panel in Fig. 3; $d_2 = 0.2$) the conical node is located at about $q_1 \approx -0.210$. This is a close-up of the eigenfunction in the second row and fourth column of Fig. 2; $d_2 = 0.4$) here, $d_1 = d_2$ and the node lies exactly on the circular conical intersection at the origin. This is a close-up of the eigenfunction ($v = 1,\ |j| = 3/2$) in the second row and fifth column of Fig. 2; $d_2 = 0.6$) the node has continued shifting further to the right and lies at about $q_1 \approx 0.225$; $d_2 = 0.8$) the node has continued shifting further to the right and lies at $q_1 \approx 0.455$. The Hamiltonian parameters in this rightmost panel match those for the adiabatic potential energy surfaces in Fig. 1.

with 2 quanta of vibration (see the discussion of perturbation theory for two-quanta states in the Supplementary Material). In this analysis, vibrational eigenstates of the 2D harmonic oscillator having definite absolute values of the vibrational angular momentum $|\ell|$ form a natural basis when the Jahn-Teller displacement for mode 1 also approaches zero. The eigenstates with 2 quanta in Fig. 2 still bear a resemblance to linear combinations of these natural basis states, which are shown for $d_2 = 0$. These analyses can also be generalized to unequal vibrational frequencies. Thus, perturbation theory shows that conical nodes can occur off the elliptical conical intersection for square-symmetric molecules.

Fig. 4 shows that the locations of nodes in nonadiabatic eigenstates vary continuously as a function of the Jahn-Teller displacement for the coupling mode. The conical intersection lies at the origin for all d_2. As d_2 increases, the vertically elongated elliptical conical node gradually approaches the origin for $d_2 = d_1$ (where it becomes circular), and then moves beyond it and becomes horizontally elongated.

For elliptical conical intersections in square-symmetric molecules, all of the energy levels are doubly degenerate, which raises the question: Are the conical nodes "accidental" in the sense that they can be removed by a change in degenerate basis? A perturbation theory analysis of the $\sigma_v = -1$ eigenstates with one vibrational quantum exactly parallels the one above and shows that their conical nodes occur at ($q_1 = +d_1,\ q_2 = 0$). Taking complex-valued linear combinations of degenerate states with $\sigma_v = \pm 1$ thus proves that the conical nodes in Fig. 3 are accidental. The doubly degenerate sets of $\sigma_v = \pm 1$ and $\sigma_d = \pm 1$ eigenstates in Fig. S3 all have conical nodes, but the nodes are on opposite sides of the conical intersection for the two eigenstates in each degenerate pair. This shows that the conical nodes for elliptical conical intersections in Fig. 2 are all accidental. The results are not particular to the symmetries chosen: Supplementary Material Fig. S5 shows many basis-set rotations of a degenerate eigenstate pair and all have the same number of conical nodes with node coordinates in one related to the node coordinates in the other by inversion through the conical intersection. These relationships between nodal coordinates within each degenerate pair are relevant for measurement of point zeroes in the total vibrational probability density (see discussion).

When $\omega_1 = \omega_2 = 200\ cm^{-1}$ and $d_1 = d_2 = 0.4$, the ($v = 2,\ |j| = 5/2$) eigenstate has a second order node [25], shown here in Fig. 2. The middle panel of Fig. 5 illustrates how this second order node arises from the simultaneous intersection of two nodal curves in the projection onto adiabatic electronic state x with two nodal curves in the projection onto y. In each projection, these nodal curves intersect at a 90° angle at the origin because of the circular symmetry of the conical intersection [25]. When this circular symmetry is broken, however, the nodal curves in each adiabatic projection need not pass through the conical intersection at the origin and need not intersect (Ref. [60] discusses non-intersecting nodal curves). As shown in the top and bottom panels of Fig. 5, the second order node separates into two first order nodes with the same sign (in Fig. 2, similar node splittings can be seen in the second and fourth columns of the third row). The splitting preserves the total electronic index for any simple closed path that encircles both conical nodes and the origin in all three cases. Supplementary Material Fig. S6 shows, for states with n = 1–5, that nth order nodes at the circularly symmetric conical intersection split into n conical nodes for slightly unequal frequencies. The first order conical nodes have the generic elliptical shape. The sum of the electronic indices for the first order nodes arising from the split equals the electronic index of the higher order parent node.

4.3. Conical node creation and annihilation via tangential nodes

Fig. 6 shows the eigenfunctions as the coupling vibration frequency is changed while the tuning vibration frequency remains fixed and the Jahn-Teller displacements remain equal. When the frequencies are equal (center column), the Hamiltonian and conical intersection have circular symmetry. Since the Jahn-Teller stabilization energy for the coupling vibration is given by $(D\omega)_2 = (1/2)\omega_2 d_2^2$, an increase (or decrease) in frequency ω_2 destroys the circular symmetry of the adiabatic potential surfaces, creating minima (or maxima) at $q_2 = \pm d_2$ on the lower surface. By stretching (or compressing) the adiabatic potential surfaces vertically along one axis, these distortions generate elliptical conical intersections for the other four columns of Fig. 6. For the nonadiabatic Hamiltonian, unequal vibrational frequencies introduce an asymmetry in the kinetic energy operator that does not occur for unequal displacements alone. Comparing the states correlated to ($v = 2,\ |j| = 1/2$) in row 5, columns 3–5 of Fig. 6 shows a node creation phenomenon not seen in Fig. 2, but the electronic index around the perimeter of each panel is stable.

As the vibrational frequency is changed, pairs of oppositely signed nodes can be created or annihilated. Fig. 7 shows an instance of this by extending the frequency difference beyond the domain shown in the top row of Fig. 6. At the frequency for which two conical nodes annihilate, there appears to be a point node where three nodal curves in the two adiabatic electronic projections cross. Around this point, the electronic character reverses sign along q_2 while remaining locally constant along q_1, so this is not a conical node. The overall electronic index for simple closed paths around this region remains 0 in all panels of Fig. 7.

This node at the point of annihilation is here referred to as a tangential node. Fig. 8 zooms into the region around this node for a frequency numerically close to annihilation. Although the intersection of three diabatic nodal curves at a single point arises by varying a

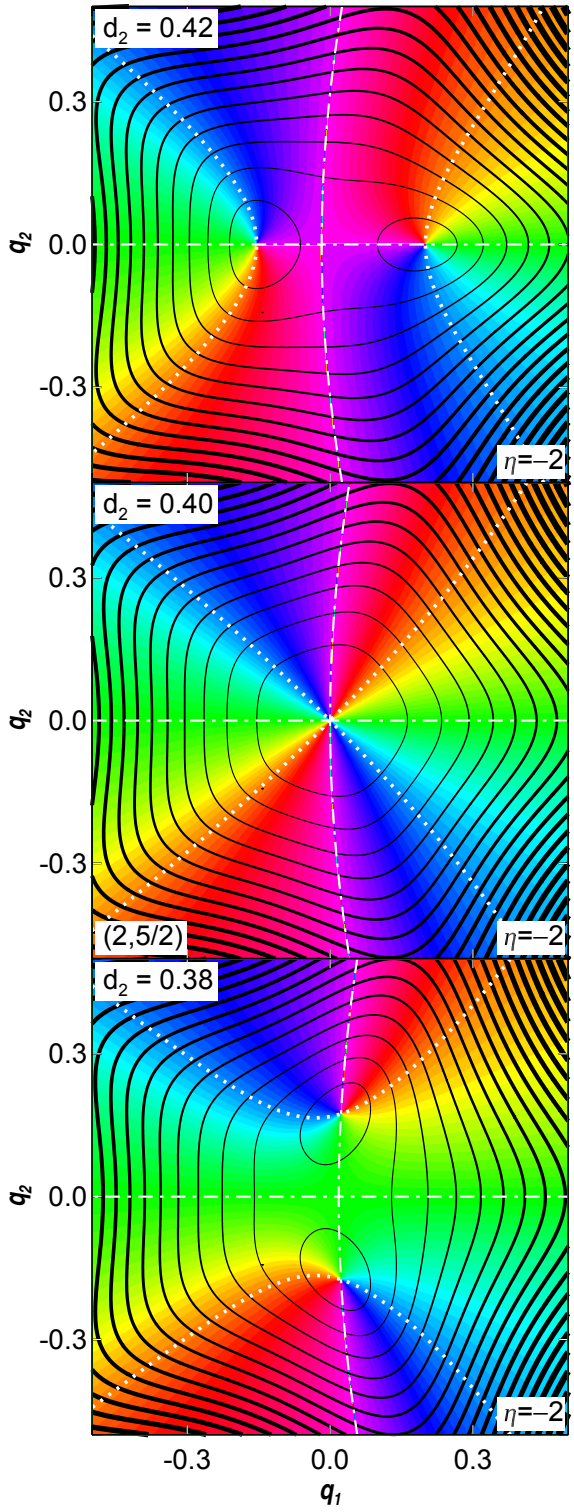

Fig. 5. Splitting of Second Order Nodes. All panels show the $\sigma_v = +1$ eigenstate correlating to ($v = 2$, $|j| = 5/2$) for parameters $\omega_1 = \omega_2 = 200\ cm^{-1}$ and $d_1 = d_2 = 0.4$, as the coupling coordinate displacement d_2 changes from panel to panel. Each panel overlays the nodal curves in the eigenfunction projections onto adiabatic electronic states x (dotted white curves) and y (dot-dashed white curves). The contour interval is 2% of each state's maximum amplitude, with thicker contours for higher amplitudes. Top) $d_2 = 0.42$ gives rise to two conical nodes with index -1 to the left and right of the origin. Middle) $d_2 = 0.4\,(=d_1)$ shows the second order node with an electronic index of -2. This second order node arises from the intersection of four nodal lines at the origin, Bottom) $d_2 = 0.38$ generates two conical nodes with electronic index -1 above and below the origin.

parameter in the presence of symmetry, the shape of this node may be typical. Along q_2, the electronic character changes sign from $+|y\rangle$ below the node to $-|y\rangle$ above the node. The even contour spacing shows that amplitude grows linearly along q_2, like a conical node. Along q_1, the electronic character is $+|x\rangle$ for all points except the node itself, where electronic character is undefined. The uneven contour spacing indicates an amplitude that grows quadratically along q_1, like a second-order node. The electronic index η is zero for any simple closed path around just this node.

The simplest generic creation/annihilation event for two oppositely signed nodes involves shifting two adiabatic vibrational nodal curves that intersect twice so that their intersections coalesce to a single point and then disappear. The two nodal curves generically become tangent at the point where they coalesce and annihilate the two conical nodes, suggesting the name tangential node. Tangential nodes are "accidental" because a parameter must be precisely tuned to the creation/annihilation event. Supplementary Material Fig. S7 shows slices through the amplitude along the tangential direction as two conical nodes annihilate. Without loss of generality in determining nodal shape, we may choose perpendicular coordinates (w, z) with the point of coalescence as the origin and the tangent line along axis w. Locally, the non-adiabatic eigenfunction can be written in terms of two orthogonal electronic basis states as

$$|\psi; w, z\rangle = (az - \alpha w^2)|A\rangle + (bz - \beta w^2)|B\rangle \tag{21}$$

This has a vibrational amplitude factor

$$\text{Þ}(w, z) = \sqrt{(az - \alpha w^2)^2 + (bz - \beta w^2)^2} \tag{22}$$

that gives the generic shape for a tangential node. The electronic factor is locally constant along the tangent line,

$$|\text{K}; w, z = 0\rangle = (-\alpha\ |A\rangle - \beta\ |B\rangle)/\sqrt{(\alpha)^2 + (\beta)^2} \tag{23a}$$

but abruptly changes sign along the perpendicular to the tangent through the origin,

$$|\text{K}; w = 0, z\rangle = \text{signum}(z)(a\ |A\rangle + b\ |B\rangle)/\sqrt{(a)^2 + (b)^2} \tag{23b}$$

Note that the electronic factors along the tangent line and its perpendicular through the origin are not generically orthogonal – their orthogonality requires $a\alpha + b\beta = 0$, which is a consequence of symmetry in Fig. 8 (with $w = q_1 - c$, $z = q_2$, $|A\rangle = |x\rangle$ and $|B\rangle = |y\rangle$, Eq. (11) requires $a = 0$ and $\beta = 0$ for $\sigma_v = +1$ states). Eq. (21) can be used to show that, in the absence of symmetry, the electronic index around a generic tangential node is zero.

Supplementary Material Fig. S8 shows that conical nodes can also be created or annihilated in a different fashion as the Hamiltonian parameters change in the presence of symmetry. This creation event for the eigenstate correlated to ($v = 2$, $|j| = 1/2$) occurs near $\omega_2 = 210.2\ \text{cm}^{-1}$ (within the range shown in Fig. 6). The intersection of three nodal curves at a single point creates two new conical nodes with the same sign as the original node and reverses the sign of the original node. As a result, the overall electronic index for simple closed paths around the region of node creation remains constant, indicating a first order singularity in the electronic factor. Even at the convergence limit of these calculations, the vibrational amplitude around the node lies between that around an adiabatic nodal curve and that around a tangential node (a hypothetical accidental first order tangential node in the presence of symmetry would not conflict with either generic accidental zeroth order tangential nodes in the absence of symmetry or symmetry-required first-order conical nodes).

Up to this point, every figure has shown a constant electronic index around the perimeter of the coordinate region plotted for each eigenstate. Fig. 9 shows how the ($v = 2$, $|j| = 3/2$) eigenstate of the circularly symmetric conical intersection changes as d_2 increases. In the circularly symmetric case (left panel), the electronic index for a path around the perimeter is $\eta = +2$. Compared to Fig. 2, the wider

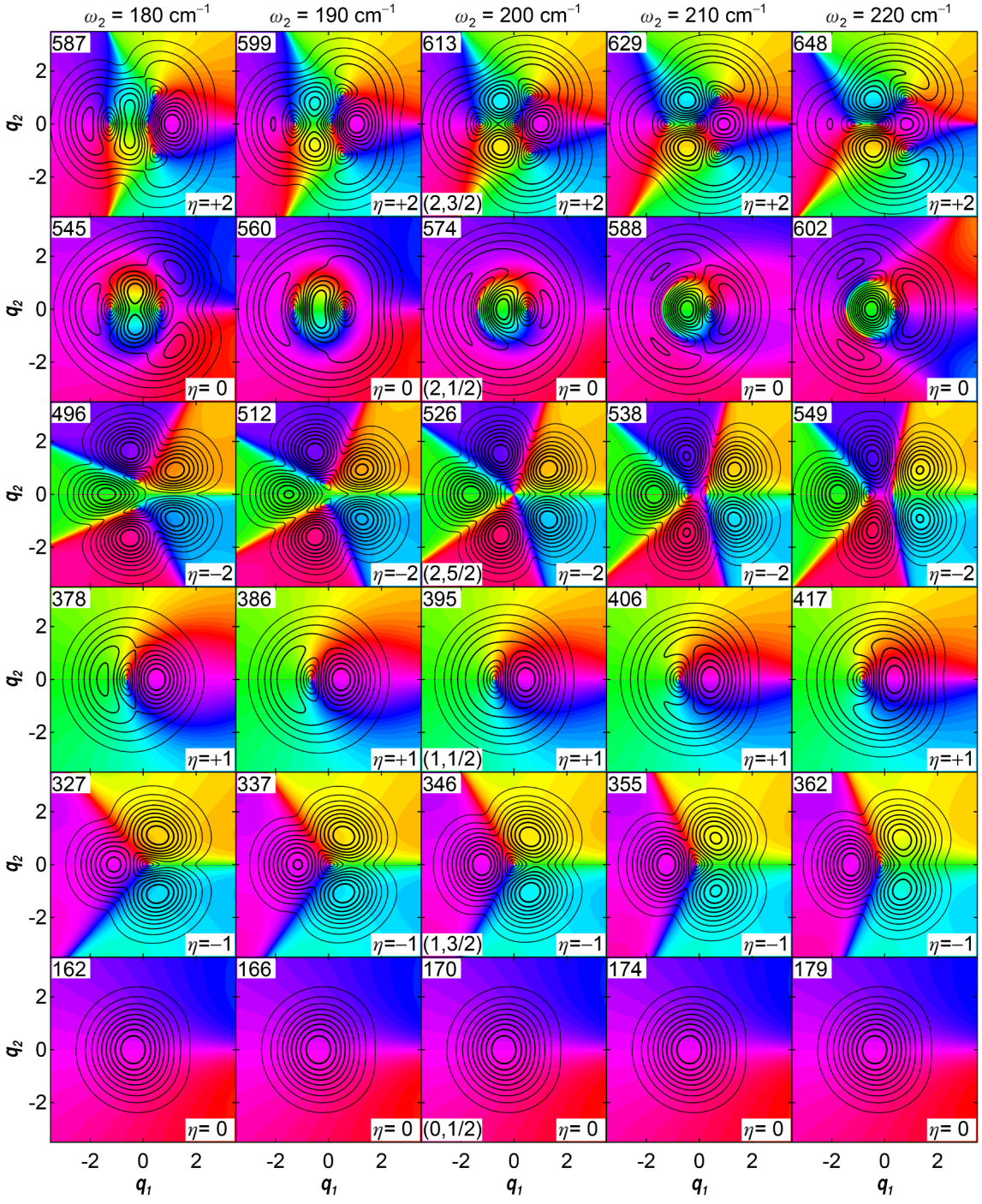

Fig. 6. Effects of varying frequency for the coupling vibration. The probability amplitude and electronic character for the six lowest energy $\sigma_v = +1$ eigenstates of the Jahn-Teller Hamiltonian are shown for vibrational frequency $\omega_1 = 200\ \mathrm{cm}^{-1}$ and $d_1 = d_2 = 0.4$. Each column has a different coupling vibration frequency ω_2 given at the top. The contour interval is 10% of the maximum probability amplitude for each state, with thicker contours for higher amplitude. Color represents electronic character as shown in the color wheel in Fig. 1. Energy eigenvalues are given in cm^{-1} at the upper left of each panel. The electronic index around the perimeter of each panel is given at lower right for each eigenfunction. The eigenfunctions in the center column match the rightmost column of Fig. 2 and have quantum numbers $(v, |j|)$ in the lower left of each panel.

coordinate range reveals that the three radial lines at $\phi = 0$, $2\pi/3$ and $4\pi/3$ approximate nodal lines at the perimeter. All four conical nodes from the left panel can be correlated throughout the three panels. For $d_2 = 0.6$, two conical nodes (circled) have moved into the range shown. Both conical nodes have an electronic index of $\eta = -1$ (see Supplementary Material Fig. S9 for close-ups), so that the electronic index around the perimeter is $\eta = 0$. For $d_2 = 0.8$, two more conical nodes with electronic index $\eta = -1$ have appeared, each along a new approximate nodal line. With 4 nodes that do not appear in the leftmost panel (node close-ups again in Fig. S9), the electronic index around the perimeter is $\eta = -2$. This shows that conical nodes can move in from (or out to) large distances from the conical intersection. These changes do not involve an obvious weakly avoided level crossing in Fig. S2, but the energy eigenvalue's curvature with d_2 suggests strong level mixing in this range.

Although nodal curves should not typically appear in nonadiabatic

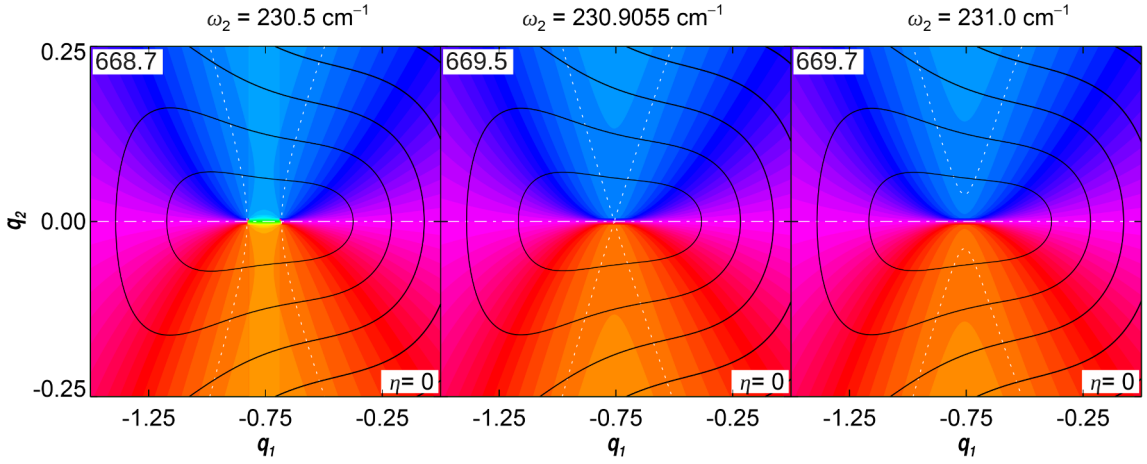

Fig. 7. Creation and Annihilation of Conical Nodes through a Tangential Node. Close-up view of the nonadiabatic eigenfunctions correlated to (v = 2, $|j|$ = 3/2) for fixed Jahn-Teller Hamiltonian parameters of ω_1= 200 cm^{-1} and $d_1 = d_2$= 0.4 as ω_2 is increased beyond the range shown in Fig. 6. Each panel overlays the nodal curves in the eigenfunction projections onto adiabatic electronic states x (dotted white curves) and y (dot-dashed white line). For each state, the contour interval is 10% of its maximum amplitude, with thicker contours for higher amplitude. Axis ranges are in a 3:1 ratio. Left) Two conical nodes still remain where nodal curves on x intersect the horizontal nodal line on y. The left and right conical nodes have electronic indices of +1 and −1, respectively. Middle) The two oppositely signed nodes combine to annihilate one another when the nodal curves on x cross each other at $\omega_2 \approx$ 230.9055 cm^{-1}. Right) Having crossed, the two nodal curves on x swap connections to avoid each other and do not cross the nodal line on y, so there are no nodes.

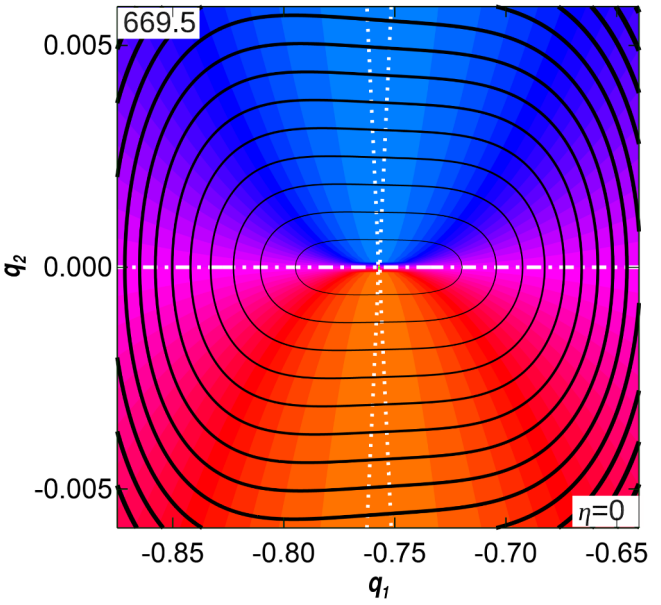

Fig. 8. Generic structure around a tangential node. A closer view of the tangential node shown in the middle panel of Fig. 7, portraying the sixth lowest eigenstate of $\sigma_v = +1$ symmetry for the Jahn-Teller Hamiltonian with ω_1=200 cm^{-1}, ω_2=230.9055 cm^{-1} and $d_1 = d_2 = 0.4$. The contour interval is 0.1% of the maximum probability amplitude, with thicker contours for higher amplitude. Color shows electronic character using the color wheel in Fig. 1. The nodal curve in the eigenfunction projection onto electronic state x is dotted white while y is dot-dashed white. Axis ranges are in a 20: 1 ratio to show the different amplitude variation along the tangential (q_1) and perpendicular (q_2) axes. The energy (cm^{-1}) is shown at upper left and the electronic index η is shown at lower right.

eigenfunctions, 7 out of the 8 conical nodes in the right panel of Fig. 9 can be connected by curves along which the amplitude never rises above 20% of the maximum amplitude. These low amplitude regions may be developing nodal curves, which suggests that conical nodes commonly occur in the weakly avoided nodal curves of eigenfunctions that are nearly adiabatic.

4.4. The role of ellipticity

Although all of the adiabatic potential surfaces considered so far have elliptical conical intersections, the symmetry equivalent minima and saddle points are obvious deformations from a simple scale transformation for one coordinate of a circular conical intersection. This raises questions about whether the amplitude at the origin is caused by the local elliptical shape of the conical intersection, global departures from an elliptical potential, or an elliptical form of the kinetic energy operator. The following considerations justify the title of this paper.

Locally circular conical intersections can be obtained by requiring that both Jahn-Teller active vibrations have the same linear coupling; $\omega_1 d_1 = \omega_2 d_2$. This still allows the Jahn-Teller stabilization energies to differ, so the adiabatic potential surfaces have minima and saddle points at the equilibrium Jahn-Teller displacements. For one Hamiltonian of this type (see Supplemental Material Fig. S10), all of the nonadiabatic eigenfunctions examined have nonzero amplitude at the conical intersection. A locally circular conical intersection is not sufficient to keep nonadiabatic eigenfunction amplitude off the conical intersection.

Purely elliptical Jahn-Teller Hamiltonians can be found by requiring that both Jahn-Teller active vibrations have the same stabilization energy; $(1/2)\omega_1 d_1^2 = (1/2)\omega_2 d_2^2 = (D\omega)$. In this case, a little algebra shows that the adiabatic potential surfaces in Eq. (4) simplify to

$$U_{\pm}(q_1, q_2) = [(1/2)\omega_1 q_1^2 + (1/2)\omega_2 q_2^2] \pm 2\sqrt{(D\omega)}\sqrt{[(1/2)\omega_1 q_1^2 + (1/2)\omega_2 q_2^2]}. \quad (24)$$

Since the level contours of $f = [(1/2)\omega_1 q_1^2 + (1/2)\omega_2 q_2^2]$ are ellipses, each elliptical contour of constant f gives one elliptical contour of constant adiabatic potential energy on each adiabatic surface: $U_{\pm} = f \pm 2\sqrt{(D\omega)}\sqrt{f}$. As a result, all contours of constant adiabatic potential energy are similar ellipses with a common center at the origin and the same eccentricity [$e = \sqrt{1 - (\omega_{min}/\omega_{max})}$ where $\omega_{min} = \min(\omega_1, \omega_2)$ and $\omega_{max} = \max(\omega_1, \omega_2)$]. Since the kinetic energy operator in the nonadiabatic Hamiltonian has the same eccentricity, equal stabilization energies create an elliptically symmetric nonadiabatic Hamiltonian. For a numerical example of a purely elliptical Jahn-Teller Hamiltonian, every nonadiabatic eigenfunction examined has nonzero amplitude at the conical intersection (see Supplementary Material Fig. S11).

For adiabatic potential surfaces, one can transform any untilted

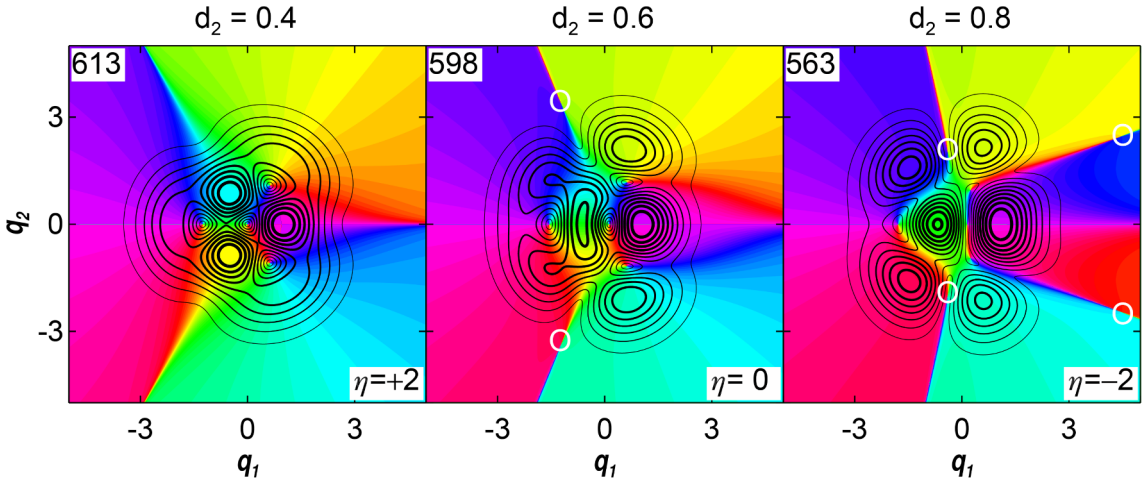

Fig. 9. Node Movements that Change the Electronic Index Around a Fixed Path. The three panels show the probability amplitude and electronic character for the sixth lowest energy $\sigma_v = +1$ eigenstate of the Jahn-Teller Hamiltonian for $\omega_1 = \omega_2 = 200\ \mathrm{cm}^{-1}$, $d_1 = 0.4$ and d_2 as specified above each panel. Contours represent 10% of the maximum probability amplitude for each state, with thicker contour lines for higher amplitude. Color represents electronic character as shown at the bottom of the color wheel in Fig. 1. The energy (cm^{-1}) for each eigenstate is shown at upper left and the electronic index around the perimeter of the area shown is at lower right. Moving from left to right, nodes enclosed in white circles have moved into the area shown and changed the electronic index around its perimeter.

elliptical 2D conical intersection into a circular 2D conical intersection by a scale transformation of one vibrational coordinate [61]. However, for non-adiabatic dynamics, ellipticity in the shape of the conical intersection cannot be transformed away because any canonical scale transformation [40] that expands a coordinate by a factor of α necessarily contracts its canonically conjugate momentum by a factor of $1/\alpha$ (this appears as an effective mass scaling in Eq. (12) of Ref. [61]). In particular, the canonical transformation $q_2' = (\omega_2/\omega_1)^{1/2} q_2$, $p_2' = (\omega_1/\omega_2)^{1/2} p_2$ transforms the above purely elliptical adiabatic potential surfaces into circular ones, but gives the nonadiabatic Hamiltonian an elliptic kinetic energy perturbation of $(1/2)[(\omega_2^2 - \omega_1^2)/\omega_1](\hat{p}_2')^2$. Similarly, transforming the purely elliptical nonadiabatic Hamiltonian to make the kinetic energy operator have the circular form $(1/2)\omega_1\left[\hat{p}_1^{\,2} + (\hat{p}_2')^2\right]$ leaves the potential surfaces elliptical. Ellipticity in *either* the potential or the kinetic energy operator makes the nonadiabatic states fundamentally different from those of a circularly symmetric nonadiabatic Hamiltonian. One could diabolically construct an apparently elliptical Hamiltonian by transformation of a circular Hamiltonian so that both the potential surfaces and the kinetic energy operator would have compensating ellipticities, but such truly circular Hamiltonians lie within an improbable lower-dimensionality sub-space in the space of purely elliptical Hamiltonians, which are themselves improbable in the higher-dimensionality space of square-symmetric Hamiltonians. Such dimensional arguments rationalize why, throughout this study, every eigenfunction calculated without global circular symmetry had nonzero amplitude at the conical intersection.

5. Discussion

Conical node points in nonadiabatic eigenfunctions have a lower dimensionality than the nodal curves in adiabatic eigenfunctions [24]. In principle, these nodes of the exact eigenfunction are observable by imaging the vibrational probability density for an eigenstate. Techniques for such imaging are discussed in Refs. [26,27]. This contrasts with conical intersections, which are a feature of the adiabatic approximation and, as such, cannot be directly observed but are calculated or inferred from their consequences. In square-symmetric molecules, the vibrational-electronic eigenstates occur in degenerate pairs and have only accidental conical nodes. Since accidental conical nodes have different vibrational coordinates for the two members of a degenerate pair, their observation in the molecular frame would require selective preparation of one eigenstate out of a degenerate pair. The vibrational imaging techniques of Refs. [27,62] involve laboratory frame measurements. Symmetry prevents a distinction between equivalent molecular frame $\hat{x}$ and $\hat{y}$ axes. Fortunately, although linearly polarized excitation from the zero point vibrational level of a totally symmetric electronic state generates $\sigma_v = +1$ states for $\hat{x}$ polarization and $\sigma_v = -1$ for $\hat{y}$ polarization, the opposite placement of accidental conical nodes with respect to the $q_1 = 0$ plane in Fig. S3 gives these degenerate state pairs the same laboratory frame vibrational probability density as each other. Similarly, the $\sigma_d = \pm 1$ states excited for $(\hat{x} \pm \hat{y})/2^{1/2}$ polarization have the same laboratory frame vibrational probability density as each other (but different from that for $\hat{x}$ or $\hat{y}$ polarization). These observations indicate that accidental conical nodes in each degenerate pair are related such that they could be observed in the lab frame.

For square-symmetric molecules with 4 equivalent atoms such as the tetra-chalcogen dications [63–65] and their isoelectronic anions [66], (which require counter-ion stabilization), gas-phase laboratory frame coordinates might be appropriately mapped using a 4-particle Dalitz plot [67,68] analogous to the 3-particle Dalitz plots used by Ref. [27] for H_3. The larger number of atoms in typical square planar molecules might eventually become accessible by improving on the spatial and temporal resolution of the surface technique used by Apkarian and co-workers [62]. Both appear to be more challenging prospects than observing essential nodes at higher symmetry conical intersections. Alternatively, conical nodes near and vibrational probability density at a conical intersection might be measurable in lower symmetry molecules such as the the radicals formed from three dissimilar alkali atoms treated by Longuet-Higgins [48].

For the elliptical conical intersections without tilt studied here, every eigenstate examined has vibrational amplitude at the conical intersection. It is well known that single-surface adiabatic eigenfunctions do not have amplitude at a conical intersection [61,69,70]. Fundamentally, this amplitude arises because the conical intersection is energetically accessible in the Hamiltonians studied here and there is no conserved pseudo-rotation angular momentum to generate a centrifugal barrier when pseudo-rotation is excited. For the circularly symmetric Jahn-Teller Hamiltonian, only eigenfunctions without a centrifugal barrier can have amplitude at the conical intersection [25], but every eigenfunction of the square-symmetric Jahn-Teller Hamiltonian can have amplitude there. The pair of studies thus leaves open questions about whether some eigenstates cannot have amplitude at the

conical intersection for intermediate symmetry Hamiltonians (e.g. groups with three-fold, five-fold, or six-fold rotations, octahedral symmetry, etc.). In the absence of such high global symmetry, the present study suggests that almost every nonadiabatic eigenstate will have amplitude on top of any energetically accessible conical intersection. Thus, conjectures by Izmaylov and co-workers [11] and by Meek and Levine [12] that nonadiabatic wavefunctions can have amplitude at a conical intersection appear to be the typical case for energetically accessible conical intersections. Such extreme examples of the dynamical Jahn-Teller effect can still generate femtosecond conical intersection dynamics in square-symmetric molecules [10,17,37], and this investigation sheds light on the eigenfunctions involved.

6. Conclusions

Elliptical conical intersections have nonadiabatic eigenstates that behave similarly to those for circular conical intersections with a few notable differences. Perturbing one frequency or one displacement from circular symmetry lowers the symmetry to D_{4h} and breaks angular symmetry, giving rise to conical intersections with an elliptical shape. As a result, nodes in the eigenstates at the conical intersection typically move off the conical intersection. This has been proven here using perturbation theory near Hougen's accidental Born-Oppenheimer case and demonstrated numerically for all other elliptical cases examined, including a nonadiabatic Hamiltonian with global elliptical symmetry.

When pseudo-rotation angular momentum symmetry is destroyed, no good quantum numbers beyond the discrete reflection symmetry eigenvalue remain. However, the integer electronic index (η) that characterizes the electronic circulation around a closed path is useful as a quantum number because it is locally stable with respect to perturbations. Oppositely-signed nodes can be created or annihilated in pairs such that η is conserved. Creation or annihilation typically occurs through a tangential node with an electronic index of 0. The vibrational amplitude surrounding a tangential node grows quadratically in the tangential direction and linearly in the perpendicular direction. For circular conical intersections, the higher order eigenfunction nodes occur at the origin with nodal lines in each electronic state converging at the conical intersection to make an n^{th} order node. For elliptical conical intersections, these nodal lines diverge to make different first order nodes, all with an electronic index of the same sign as each other and as the original n^{th} order node, maintaining the electronic index η. The formation of adiabatic nodal curves appears to involve expansion and coalescence of conical nodes, which can make the electronic index difficult to evaluate as it ultimately becomes ill-defined in the adiabatic limit. Although the electronic index is stable with respect to small perturbations, it is not globally conserved.

None of these nodes found here occur at the conical intersection, so all eigenfunctions can have probability amplitude at the conical intersection as long as the conical intersection is energetically accessible. Depending on the degenerate eigenstate selected, the conical nodes are located at different coordinates, so they are accidental in nature and disappear for complex-valued linear combinations of degenerate eigenstates. Conical nodes were observed for all sets of real-valued eigenstates here. While accidental nodes shifted off the conical intersection may be experimentally difficult to observe, the conclusion that all eigenstates have amplitude at the conical intersection is experimentally testable.

Acknowledgments

This material is based upon work supported by the National Science Foundation under Grants No. CHE-1405050 and CHE-1800523. Any opinions, findings, and conclusions or recommendations expressed in this material are those of the authors and do not necessarily reflect the views of the National Science Foundation.

Appendix A. Supplementary data

Supplementary data to this article can be found online at https://doi.org/10.1016/j.chemphys.2019.01.004.

References

[1] E. Teller, Internal conversion in polyatomic molecules, Israel J. Chem. 7 (1969) 227–235.
[2] H. Koppel, W. Domcke, L.S. Cederbaum, Multimode molecular-dynamics beyond the Born-Oppenheimer approximation, Adv. Chem. Phys. 57 (1984) 59–246.
[3] J.W. Zwanziger, E.R. Grant, Topological phase in molecular bound states: application to the E⊗e system, J. Chem. Phys. 87 (1987) 2954–2964.
[4] M. Klessinger, J. Michl, Excited States and Photochemistry of Organic Molecules, VCH Publishers, New York, 1995.
[5] D.R. Yarkony, Diabolical conical intersections, Rev. Mod. Phys. 68 (1996) 985–1013.
[6] M.A. Robb, M. Olivucci, Photochemical processes: potential energy surface topology and rationalization using VB arguments, J. Photochem. Photobiol. A 144 (2001) 237–243.
[7] D.G. Truhlar, C.A. Mead, Relative likelihood of encountering conical intersections and avoided crossings on the potential energy surfaces of polyatomic molecules, Phys. Rev. A 68 (2003) 032501.
[8] J.D. Coe, T.J. Martinez, Competitive decay at two- and three-state conical intersections in excited-state intramolecular proton transfer, J. Am. Chem. Soc. 127 (2005) 4560–4561.
[9] S. Matsika, P. Krause, Nonadiabatic events and conical intersections, Annu. Rev. Phys. Chem. 62 (2011) 621–643.
[10] D.M. Jonas, Vibrational and nonadiabatic coherence in 2D electronic spectroscopy, the Jahn-Teller effect and energy transfer, Annu. Rev. Phys. Chem. 69 (2018) 327–352.
[11] I. Ryabinkin, L. Joubert-Doriol, A.F. Izmaylov, When do we need to account for the geometric phase in excited state dynamics? J. Chem. Phys. 140 (2014) 214116.
[12] G.A. Meek, B.G. Levine, Wave function continuity and the diagonal Born-Oppenheimer correction at conical intersections, J. Chem. Phys. 144 (2016) 184109.
[13] H.C. Longuet-Higgins, U. Öpik, M.H.L. Pryce, R.A. Sack, Studies of the Jahn-Teller effect II. The dynamical problem, Proc. R. Soc. Lond. A 244 (1958) 1–16.
[14] B.E. Applegate, T.A. Barckholtz, T.A. Miller, Explorations of conical intersections and their ramifications for chemistry through the Jahn-Teller effect, Chem. Soc. Rev. 32 (2003) 38–49.
[15] H.A. Jahn, E. Teller, Stability of Polyatomic Molecules in Degenerate Electronic States. I. Orbital Degeneracy, Proc. R. Soc. London Ser. A 161 (1937) 220–235.
[16] J. McCusker, Femtosecond absorption spectroscopy of transition metal charge-transfer complexes, Acc. Chem. Res. 36 (2003) 876–887.
[17] D.A. Farrow, W. Qian, E.R. Smith, A.A. Ferro, D.M. Jonas, Polarized pump-probe measurements of electronic motion via a conical intersection, J. Chem. Phys. 128 (2008) 144510.
[18] J.T. Hougen, Vibronic interactions in molecules with a fourfold symmetry axis, J. Mol. Spectrosc. 13 (1964) 149–167.
[19] M. Gouterman, Electronic spectra, in: D. Dolphin (Ed.), The Porphyrins, Academic Press, New York, 1978, pp. 1–156.
[20] G. Hunter, Conditional probability amplitudes in wave mechanics, Int. J. Quantum Chem. 9 (1975) 237–242.
[21] A. Abedi, N.T. Maitra, E.K.U. Gross, Exact factorization of the time-dependent electron-nuclear wave function, Phys. Rev. Lett. 105 (2010) 123002.
[22] L.S. Cederbaum, The exact molecular wavefunction as a product of an electronic and a nuclear wavefunction, J. Chem. Phys. 138 (2013) 224110.
[23] W.K. Peters, V. Tiwari, D.M. Jonas, Nodeless vibrational amplitudes and quantum nonadiabatic dynamics in the nested funnel for a pseudo Jahn-Teller molecule or homodimer, J. Chem. Phys. 147 (2017) 194306.
[24] P.W. Foster, W.K. Peters, D.M. Jonas, Nonadiabatic eigenfunctions can have conical nodes, Chem. Phys. Lett. 683 (2017) 268–275.
[25] P.W. Foster, D.M. Jonas, Nonadiabatic eigenfunctions can have amplitude, signed conical nodes, or signed higher order nodes at a conical intersection with circular symmetry, J. Phys. Chem. A 121 (2017) 7401–7413.
[26] L.P.H. Schmidt, T. Jahnke, A. Czasch, M. Schoffler, H. Schmidt-Bocking, R. Dorner, Spatial imaging of the H_2^+ vibrational wave function at the quantum limit, Phys. Rev. Lett. 108 (2012) 073202.
[27] P.C. Fechner, H. Helm, Imaging of spatial many-body wave functions via linear momentum measurements, Phys. Chem. Chem. Phys. 16 (2014) 453–457.
[28] J. Czub, L. Wolniewicz, On the non-adiabatic potentials in diatomic-molecules, Mol. Phys. 36 (1978) 1301–1308.
[29] G. Hunter, Nodeless wave-functions and spiky potentials, Int. J. Quantum Chem. 19 (1981) 755–761.
[30] N.I. Gidopoulos, E.K.U. Gross, Electronic non-adiabatic states: towards a density functional theory beyond the Born-Oppenheimer approximation, Philos. Trans. R. Soc. A 372 (2014) 20130059.
[31] I. Ryabinkin, A.F. Izmaylov, Geometric phase effects in dynamics near conical intersections: symmetry breaking and spatial localization, Phys. Rev. Lett. 111 (2013) 220406.
[32] C. Xie, B.K. Kendrick, D.R. Yarkony, H. Guo, Constructive and destructive interference in nonadiabatic tunneling via conical intersections, J. Chem. Theory Comput. 13 (2017) 1902–1910.

[33] C. Xie, D.R. Yarkony, H. Guo, Nonadiabatic tunneling via conical intersections and the role of the geometric phase, Phys. Rev. A 95 (2017) 022104.
[34] G.H. Herzberg, Electronic Spectra of Polyatomic Molecules, Krieger, Malabar, FL, 1991.
[35] J.A. Shelnutt, X.-Z. Song, J.-G. Ma, S.-L. Jia, W. Jentzena, C.J. Medforth, Nonplanar porphyrins and their significance in proteins, Chem. Soc. Rev. 27 (1998) 31–41.
[36] D.A. Farrow, E.R. Smith, W. Qian, D.M. Jonas, The polarization anisotropy of vibrational quantum beats in resonant pump-probe experiments: diagrammatic calculations for square symmetric molecules, J. Chem. Phys. 129 (2008) 174509.
[37] K.A. Kitney-Hayes, A.W. Albrecht-Ferro, V. Tiwari, D.M. Jonas, Two-dimensional Fourier transform electronic spectroscopy at a conical intersection, J. Chem. Phys. 140 (2014) 124312.
[38] J.E. Marsden, A.J. Tromba, Vector Calculus, W. H. Freeman, San Francisco, 1981.
[39] D. Papousek, M.R. Aliev, Molecular Vibrational-Rotational Spectra, Elsevier Scientific, New York, 1982.
[40] H. Goldstein, Classical Mechanics, second ed., Addison-Wesley, Reading, MA, 1980.
[41] D.R. Yarkony, Conical intersections: the new conventional wisdom, J. Phys. Chem. A 105 (2001) 6277–6293.
[42] E.R. Smith, D.A. Farrow, D.M. Jonas, Response functions for dimers and square symmetric molecules in four-wave-mixing experiments with polarized light, J. Chem. Phys. 123 (2005) 044102.
[43] E.R. Smith, D.A. Farrow, D.M. Jonas, Publisher's Note: "Response functions for dimers and square symmetric molecules in four-wave-mixing experiments with polarized light" [J. Chem. Phys. 123, 044102 (2005)], J. Chem. Phys. 123 (2005) 179902.
[44] E.R. Smith, D.A. Farrow, D.M. Jonas, Erratum: "Response functions for dimers and square symmetric molecules in four-wave-mixing experiments with polarized light" [J. Chem. Phys. 123, 044102 (2005)], J. Chem. Phys. 128 (2008) 109902.
[45] S. Sunder, H.J. Bernstein, The vibrational spectra of the metalloporphyrins: a normal coordinate analysis of the planar vibrations in the Cu-chelates of porphin, porphin-d_4 (*meso*), 1:3:5:7-tetramethyl porphin and 1:2:3:4:5:6:7:8-octamethyl porphin, J. Raman Spectrosc. 5 (1976) 351–371.
[46] W. Moffitt, A.D. Liehr, Configurational instability of degenerate electronic states, Phys. Rev. 106 (1957) 1195–1200.
[47] M. Born, K. Huang, Dynamical Theory of Crystal Lattices, Clarendon Press, Oxford, 1962.
[48] H.C. Longuet-Higgins, The intersection of potential energy surfaces in polyatomic molecules, Proc. R. Soc. Lond. A 344 (1975) 147–156.
[49] C.A. Mead, D.G. Truhlar, On the determination of Born-Oppenheimer nuclear motion wave functions including complications due to conical intersections and identical nuclei, J. Chem. Phys. 70 (1979) 2284–2296.
[50] R.N. Bracewell, The Fourier Transform and Its Applications, third ed., McGraw Hill, Boston, 2000.
[51] H.C. Longuet-Higgins, Some recent developments in the theory of molecular energy levels, in: H. Thompson (Ed.), Advances in Spectroscopy, Interscience Publishers Inc, New York, 1961, pp. 429–472.
[52] G. Herzberg, H.C. Longuet-Higgins, Intersection of potential energy surfaces in polyatomic molecules, Discuss. Faraday Soc. 35 (1963) 77–82.
[53] M.V. Berry, Quantal phase factors accompanying adiabatic changes, Proc. R. Soc. Lond. A 392 (1984) 45–57.
[54] P.R. Bunker, Molecular Symmetry and Spectroscopy, Academic Press Inc, Orlando, 1979.
[55] L.D. Landau, E.M. Lifschitz, Quantum Mechanics, third ed., Pergamon Press, New York, 1977.
[56] T.C. Thompson, D.G. Truhlar, C.A. Mead, On the form of the adiabatic and diabatic representation and the validity of the adiabatic approximation for X_3 Jahn-Teller systems, J. Chem. Phys. 82 (1985) 2392–2407.
[57] B.N. Parlett, The Symmetric Eigenvalue Problem, Prentice-Hall, Englewood Cliffs, NJ, 1980.
[58] B.R. Judd, Exact solutions to a class of Jahn-Teller systems, J. Phys. C: Solid State Phys. 12 (1979) 1685–1692.
[59] C. Cohen-Tannoudji, B. Diu, F. Lalöe, Quantum Mechanics, Wiley-Interscience, Paris, 1977.
[60] R. Courant, D. Hilbert, Methods of Mathematical Physics, first English ed., Wiley-Interscience, 1953.
[61] D.R. Yarkony, Nuclear dynamics near conical intersections in the adiabatic representation: I. The effects of local topography on interstate transitions, J. Chem. Phys. 114 (2001) 2601–2613.
[62] J. Lee, S.M. Perdue, A.R. Perez, P.Z. El-Khoury, K. Honkala, V.A. Apkarian, Orbiting orbitals: visualization of vibronic motion at a conical intersection, J. Phys. Chem. A 117 (2013) 11655–11664.
[63] G. Cardinal, R.J. Gillespie, J.F. Sawyer, J.E. Vekris, Charge-transfer interactions in the square-planar chalcogen cations, M_4^{2+} : preparation and crystal-structures of the compounds $(Se_4^{2+})(Sb_2F_4^{2+})(Sb_2F_5^{+})(SbF_6^{-})_5$,$(Se_4^{2+})(AlCl_4^{-})_2$, and $(Te_4^{2+})(SbF_6^{-})_2$, J. Chem. Soc.-Dalton Trans. (1982) 765–779.
[64] M.W. Wong, Quantum-chemical calculations of sulfur-rich compounds, Top. Curr. Chem. 231 (2003) 1–31.
[65] B.M. Elliott, A.I. Boldyrev, Ab initio probing of the aromatic oxygen cluster O_4^{2+}, J. Phys. Chem. A 109 (2005) 236–239.
[66] J.D. Corbett, Polyatomic Zintl anions of the post-transition elements, Chem. Rev. 85 (1985) 383–397.
[67] M. Schulz, D. Fischer, T. Ferger, R. Moshammer, J. Ullrich, Four-particle Dalitz plots to visualize atomic break-up processes, J. Phys. B-At. Mol. Opt. Phys. 40 (2007) 3091–3099.
[68] M.F. Ciappina, M. Schulz, T. Kirchner, D. Fischer, R. Moshammer, J. Ullrich, Double ionization of helium by ion impact analyzed using four-body Dalitz plots, Phys. Rev. A 77 (2008) 12.
[69] C.A. Mead, Electronic Hamiltonian, wave functions, and energies, and derivative coupling between Born-Oppenheimer states in the vicinity of a conical intersection, J. Chem. Phys. 78 (1983) 807–814.
[70] A.J.C. Varandas, Z.R. Xu, On the behavior of single surface nuclear wavefunctions in the vicinity of the conical intersection for an X_3 system, Chem. Phys. Lett. 316 (2000) 248–256.

Supplementary Material

for

Nonadiabatic conical nodes are near but not at an elliptical conical intersection

Peter W. Foster and David M. Jonas

Department of Chemistry

and

Renewable and Sustainable Energy Institute

University of Colorado, Boulder, Colorado 80309 USA

Overview of Eigenstates for Circular Conical Intersections

The circular symmetry Jahn-Teller Hamiltonian has three parameter regimes with simple expressions for the energy eigenvalues.[1] The half-odd integral pseudo-rotation quantum number *j* is rigorously conserved across all three parameter regimes. For small Jahn-Teller displacements, the 2D harmonic oscillator vibrational quantum number v is good and the energy levels are well approximated by perturbation theory.[1, 2] The perturbation theory expression involves three quantum numbers: the 2D harmonic oscillator vibrational quantum number v and vibrational angular momentum ℓ plus an electronic angular momentum $\lambda = \pm 1$ that couple to give the pseudo-rotation quantum number $j = \ell + (\lambda / 2)$. The energy eigenvalues are given by $E = \omega(v+1) - 2(D\omega)[\ell\lambda + 1]$.[2] As d increases, all three electronic and vibrational quantum numbers break down through $j-$ conserving avoided crossings.[3, 4] Before a level undergoes its first avoided crossing, the small Jahn-Teller displacement quantum numbers $(v, |j|)$ remain good. For larger displacements, the lower eigenvalues approximate those of a double-valued radial potential $V^d(r) = (1/2)\omega(r-d)^2$ with half-odd integral pseudo-rotation quantum numbers. In this regime, the eigenvalues are $E = \omega(p+1/2) - (D\omega) + \omega j^2/(2d^2)$, where the radial vibrational quantum number *p* is a non-negative integer (Eq. (6.16) of ref. [1] defines *p* differently). Since radial curve crossing between the lower and upper adiabatic potentials is unhindered at the origin in this model, it has diabatic aspects. At very large displacements, the low energy eigenstates become vibrational eigenstates of the lower adiabatic potential (the hat) and the pseudo-rotation term in the energy tends to zero.[1] For any given vibrational eigenstate of the hat, this transition involves a finite number of avoided crossings. After a level's last avoided crossing, its adiabatic quantum numbers $(p, |j|)$ become good. Since the vibronic eigenstates of the upper adiabatic potential (the cone) are embedded among the higher energy vibrational eigenstates of the hat, an endless series of avoided crossings prevents convergence to adiabatic behavior as the Jahn-Teller displacement increases.[3] Nonetheless, for specific Jahn-Teller displacements, some eigenstates are predominantly on the cone. [3]

label	Circular Quantum Numbers		Judd's Quantum Numbers		k^2 (Judd) or d^2 (here)	Jahn-Teller Stabilization Energy ($D\omega$) for ω = 200 cm^{-1}	Analytical Eigenvalue (cm^{-1})	Numerical Eigenvalues (cm^{-1})	Errors (10^{-12} cm^{-1})
	v	j	v	m					
y	1	3/2	1	1	5/8	62.500000000000	237.500000000000	237.499999999994	−6
								237.499999999999	−1
z	2	5/2	1	2	21/8	262.500000000000	37.500000000000	37.500000000007	0.7
								37.500000000018	1.8
w	2	3/2	2	1	$(27/32) + ((1009)^{1/2}/32)$	183.639876089179	316.360123910821	316.360123910819	−2
								316.360123910825	4
x	3	5/2	2	2	$(75/32) + ((4113)^{1/2}/32)$	434.789609310300	65.2103906897004	65.2103906897046	4.2
								65.2103906897078	7.4
u	2	5/2	2	2	$(75/32) - ((4113)^{1/2}/32)$	33.9603906897004	466.039609310300	466.039609310297	−3
								466.039609310298	−2
v	3	7/2	2	3	$(147/32) - ((9729)^{1/2}/32)$	151.138458322995	348.861541677005	348.861541676996	−9
								348.861541676997	−8
t	3	3/2	3	1	$(19/16) + p + (269/(256p))$ where $p = ((4867 + (4222580)^{1/2})/4096)^{1/3}$	326.079876508688	373.920123491312	373.920123491315	3
								373.920123491316	4
s	4	5/2	3	2	$(74941/5184)^{1/2}\cos(\kappa) + (347/144)$ where $\cos(3\kappa) = 17105435/(74941)^{3/2}$	613.982855981044	86.0171440189559	86.0171440189474	−8.5
								86.0171440189597	3.8
r	5	7/2	3	3	$(167149/5184)^{1/2}\cos(\xi) + (611/144)$ where $\cos(3\xi) = 48524723/(167149)^{3/2}$	972.994449879604	−272.994449879604	−272.994449879601	−3
								−272.994449879599	−5

Table S1: Comparison to Analytic Eigenvalues for Circular Conical Intersections

For circular conical intersections with special ratios of the Jahn-Teller stabilization energy to vibrational frequency, Judd obtained an analytic expression for some isolated eigenvalues.[5] Judd used an angular quantum number $m = |j| - 1/2$ and a baseline quantum number v that does not have a simple relation to the eigenfunction. Eq. (10) of Judd's paper gives some isolated analytic energy eigenvalues as $E(v) = \omega(v + 1/2) - (D\omega)$, where v is Judd's baseline quantum number. Table S1 compares the numerical eigenvalues obtained here by truncated Hamiltonian diagonalization with all nine analytic eigenvalues in Table 2 of ref. [5] for the $E \otimes e$ Jahn-Teller system. The states Judd labeled '*x*' and '*u*' are separately correlated with their stabilization energies based on Figure 2 of Judd's paper. Comparing their coordinates in Table 2 and Figure 2 of Judd's paper, it is clear that the states labeled '*r*' and '*s*' have been qualitatively mis-positioned in Judd's Figure 2, where they should lie at the lower right range of the plot (large stabilization energy, small energy) instead of the upper left (small stabilization energy, large energy). As a result, the small stabilization energy circular quantum number assignments suggested by Judd's Figure 2 are incorrect ['*r*' ≠ (*v*=3,|*j*|=7/2) and '*s*' ≠ (*v*=3,|*j*|=5/2)], and the assignments for these two states are based on Fig. S1. All other quantum number assignments are based on following the eigenvalue curves in Judd's Figure 2 back to small stabilization energies, where perturbation theory Eq. (7) of ref. [2] connects the energy to the quantum numbers. In Table S1, the ratio $(D\omega)/\omega$ of Jahn-Teller stabilization energy to vibrational frequency ranges from ~1/6 to ~5 and the quantum numbers go as high as $(v = 5, |j| = 7/2)$. For the vibrational frequency of $\omega =$ 200 cm^{-1} used in Table S1, the eigenvalues are typically a few hundred cm^{-1} and all errors are less than 10^{-11} cm^{-1}. Errors typically occur only in the 15th digit, as measured either by discrepancies with Judd's analytic results or by departures from numerical degeneracy.

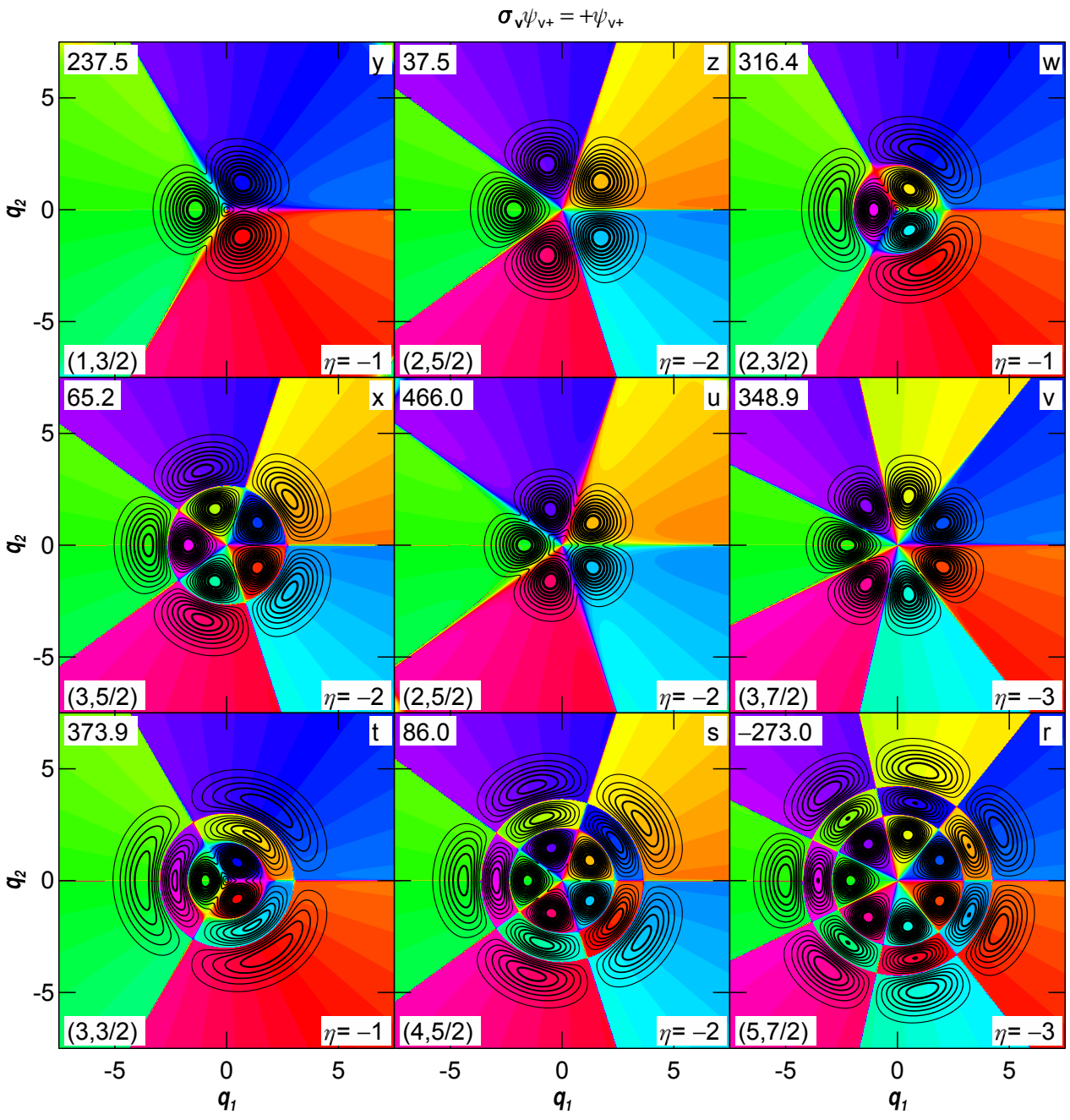
$\sigma_v\psi_{v+} = +\psi_{v+}$
237.5
y
(1,3/2)
η= –1
37.5
z
(2,5/2)
η= –2
316.4
w
(2,3/2)
η= –1
65.2
x
(3,5/2)
η= –2
466.0
u
(2,5/2)
η= –2
348.9
v
(3,7/2)
η= –3
373.9
t
(3,3/2)
η= –1
86.0
s
(4,5/2)
η= –2
–273.0
r
(5,7/2)
η= –3
q_2
q_1
5
0
-5

Figure S1

Figure S1: Nonadiabatic Eigenfunctions with Analytic Eigenvalues

The nine panels here show the nonadiabatic eigenfunctions for the $\sigma_v = \pm 1$ eigenstates with exact eigenvalues in Table S1. For each eigenfunction, the energy eigenvalue (cm^{-1}) is given at upper left, Judd's label at upper right, the small Jahn-Teller displacement circular quantum numbers $(v, |j|)$ from Table S1 at lower left, and the electronic index around the perimeter at lower right. The v quantum number is assigned based on eigenfunction appearance so that $v-(|j|-1/2)$ gives the number of radial nodes (such assignments jump through avoided crossings). In each panel, the contour interval is 10% of the maximum probability amplitude for that state, with thicker contour lines for higher amplitude. The color wheel in Figure 1 is used to represent electronic character. Note that each eigenfunction in this figure arises from a different Hamiltonian, which is specified in Table S1 according to the label at upper right. Comparing the angular dependence of the eigenstate colors to those for the lower adiabatic electronic state in Figure 1 of ref. [2] indicates that all of these eigenstates are predominantly on the lower adiabatic potential surface (the hat state).

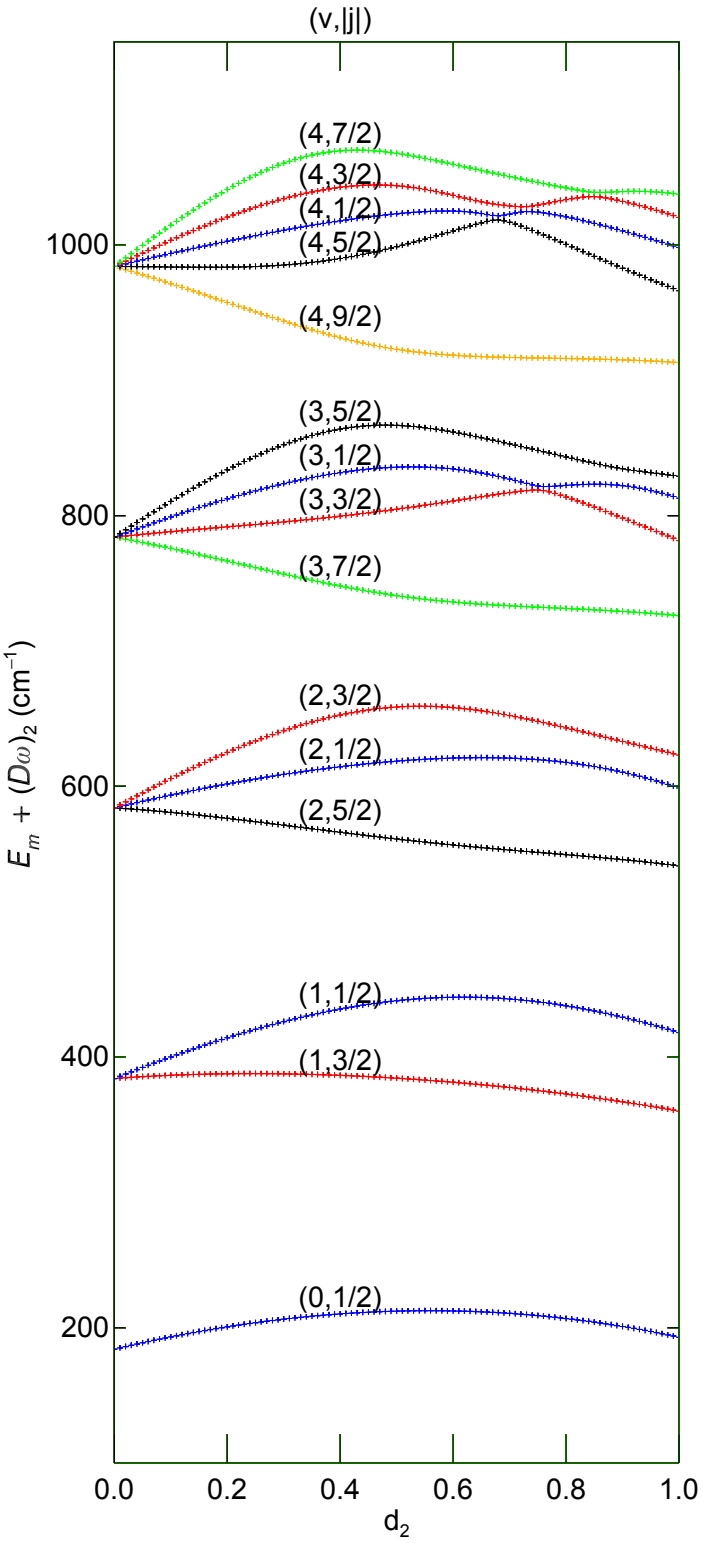
(v,|j|)
(4,7/2)
(4,3/2)
(4,1/2)
(4,5/2)
(4,9/2)
(3,5/2)
(3,1/2)
(3,3/2)
(3,7/2)
(2,3/2)
(2,1/2)
(2,5/2)
(1,1/2)
(1,3/2)
(0,1/2)
1000
800
600
400
200
0.0
0.2
0.4
0.6
0.8
1.0
d2
Em + (Dω)2 (cm-1)

Figure S2

Figure S2: Energy Eigenvalues as a Function of Displacement for Mode 2

The energy eigenvalues for the 15 lowest pairs of eigenstates are shown for the Jahn-Teller Hamiltonian with $\omega_1 = \omega_2 = 200$ cm^{-1} and $d_1 = 0.4$ as a function of d_2 from 0 to 1 (stepsize is 0.01). To show relative trends more clearly, the vertical axis is the sum of the eigenstate energy E_m and the Jahn-Teller stabilization energy $(D\omega)_2 = (1/2)\omega_2 d_2^2$. The quantum numbers v and $|j|$ for the eigenstates are specified at $d_2 = 0.4$ where the conical intersection has circular symmetry and the pseudo-rotation quantum number j is rigorous. The marker color indicates the correlation to $|j|$ at circular symmetry: blue for $|j| = 1/2$, red for $|j| = 3/2$, black for $|j| = 5/2$, green for $|j| = 7/2$, and orange for $|j| = 9/2$. Several avoided crossings can be seen, including weakly avoided crossings between eigenvalues labelled (4,5/2) and (4,1/2); (4,1/2) and (4,3/2); (4,3/2) and (4,7/2); (3,3/2) and (3,1/2); crossing between (3,1/2) and (3,5/2) appears to be more strongly avoided. The quantum numbers characteristic of each eigenfunction can be determined by pretending each weakly avoided crossing is an actual crossing, so the quantum numbers do not necessarily correlate with marker color beyond $d_2 \approx$ 0.6.

Quantum Numbers in Circular Symmetry		Numerical Energy Eigenvalues (cm^{-1}) for $\omega_1 = \omega_2 = 200$ cm^{-1}, $d_1 = 0.4$ and d_2 specified					
v	j	$d_2 = 0$	$d_2 = 10^{-10}$	$d_2 = 0.2$	$d_2 = 0.4$	$d_2 = 0.6$	$d_2 = 0.8$
0	1/2	184.000000000000	184.000000000000	180.565095246248	170.125283738329	152.320722683800	126.694700417582
0	1/2	184.000000000000	184.000000000002	180.565095246250	170.125283738333	152.320722683800	126.694700417582
1	3/2	383.999999999999	383.999999993183	367.541999592926	346.342118067196	321.269765036856	292.594240084540
1	3/2	384.000000000000	383.999999993183	367.541999592927	346.342118067199	321.269765036857	292.594240084542
1	1/2	384.000000000000	384.000000006818	394.141673298400	395.369313113912	384.064650690666	357.740380346399
1	1/2	384.000000000000	384.000000006819	394.141673298404	395.369313113912	384.064650690668	357.740380346402
2	5/2	583.999999999999	583.999999987410	556.252387494798	525.963160943148	496.590888122214	469.426835580456
2	5/2	584.000000000000	583.999999987410	556.252387494799	525.963160943152	496.590888122215	469.426835580458
2	1/2	584.000000000000	583.999999999997	581.692342934045	574.396095014677	560.788974834820	537.599367538494
2	1/2	584.000000000002	584.000000000000	581.692342934046	574.396095014679	560.788974834823	537.599367538495
2	3/2	584.000000000004	584.000000012592	604.984709138495	612.654738041824	598.069711514026	563.101895663671
2	3/2	584.000000000005	584.000000012593	604.984709138498	612.654738041825	598.069711514027	563.101895663671
3	7/2	783.999999999999	783.999999982460	746.286233909557	707.839312281093	676.047227088426	651.312249855972
3	7/2	784.000000000000	783.999999982461	746.286233909559	707.839312281098	676.047227088432	651.312249855975
3	3/2	784.000000000000	783.999999994458	771.634718813502	759.517876813196	750.750781167499	742.279607372564
3	3/2	784.000000000000	783.999999994459	771.634718813502	759.517876813199	750.750781167500	742.279607372565
3	1/2	784.000000000001	784.000000005540	792.356753806846	791.702492762055	774.365833853301	733.608848747555
3	1/2	784.000000000001	784.000000005541	792.356753806848	791.702492762055	774.365833853303	733.608848747557
3	5/2	784.000000000003	784.000000017538	813.756121342917	823.878877562159	801.595570372299	763.231620902958
3	5/2	784.000000000005	784.000000017539	813.756121342918	823.878877562160	801.595570372300	763.231620902963

Table S2: Energy Eigenvalues for Different Displacements of Mode 2

Numerical eigenvalues for the twenty lowest energy eigenstates of Jahn-Teller Hamiltonians with $\omega_1 = \omega_2 = 200$ cm^{-1}, $d_1 = 0.4$ and displacements d_2 tabulated above each column. These eigenvalues include all states shown in Figures 2-5 of the main paper and Figures S3-S5 of the supplementary material. Quantum numbers are assigned to eigenvalues based on eigenfunction appearance, which agrees with assignment based on continuous energy eigenvalue correlation except for $(v = 3, |j| = 3/2)$ and $(v = 3, |j| = 1/2)$ at $d_2 =$ 0.8 (Fig. S2 shows these two levels undergo an avoided crossing between $d_2 =$ 0.6 and 0.8). Symmetry required degeneracies are maintained to 15 digits. The numerical eigenvalues for $d_2 = 0$ (accidental Born-Oppenheimer case) exhibit 15 digit accuracy vs. the analytic formula $E(v_1, v_2) = \omega_1(v_1 + 1/2) + \omega_2(v_2 + 1/2) - (D\omega)_1$, where $(D\omega)_1 = (1/2)\omega_1 d_1^2$ = 16 cm^{-1}. Numerical eigenvalues for $d_2 =$ 10^{-10} match degenerate first order perturbation theory expressions [see Eq. (20) of the main text and the discussion following Fig. S4 below] for the $v =$ 0, 1, and 2 energies to 15 digit accuracy.

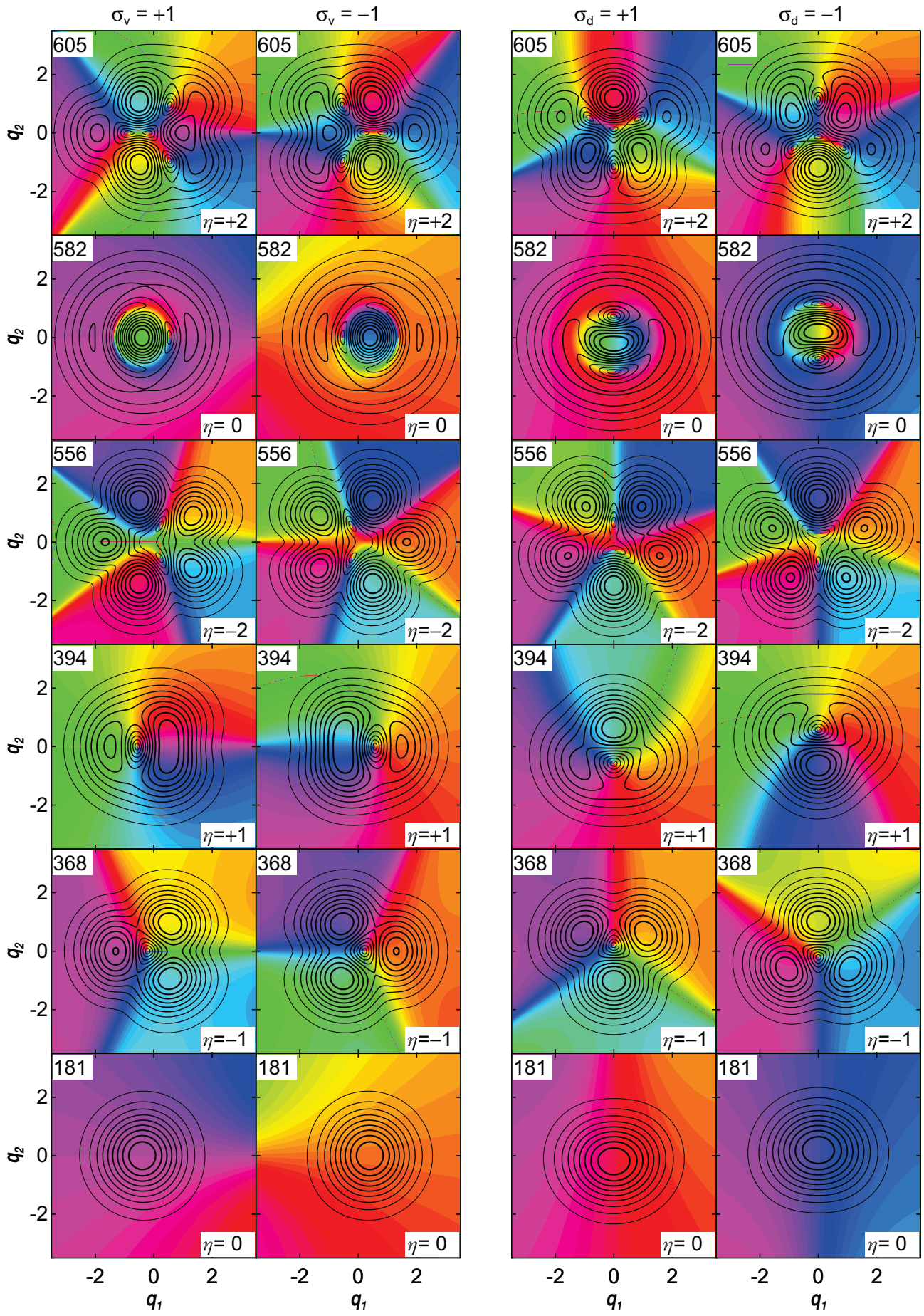
σv = +1
σv = −1
σd = +1
σd = −1
605
582
556
394
368
181
η=+2
η= 0
η=−2
η=+1
η=−1
q2
q1
-2
0
2

Figure S3: Real-valued Eigenfunctions for All σ_v and σ_d Eigenvalues

The four columns each have six panels showing the probability amplitude and electronic character of the six lowest energy eigenstates with a given reflection symmetry for the Jahn-Teller Hamiltonian with vibrational frequencies $\omega_1 = \omega_2 = 200$ cm^{-1} and Jahn-Teller displacements $d_1 = 0.4$ and $d_2 = 0.2$. The left column has $\sigma_v = +1$ symmetry, the second column has $\sigma_v = -1$ symmetry, the third column has $\sigma_d = +1$ symmetry, and the right column has $\sigma_d = -1$ symmetry. In each panel, the contour interval is 10% of the maximum probability amplitude for that state, with thicker contour lines for higher amplitude. The color wheel in Figure 1 is used to represent electronic character. In each column, the lowest energy state is on the bottom and energy increases upward. In each panel, the label at upper left gives the eigenstate energy in wavenumbers and the label at lower right specifies the electronic index η around the perimeter of each panel. η is constant for each row, while the location of the nodes is different between the paired columns.

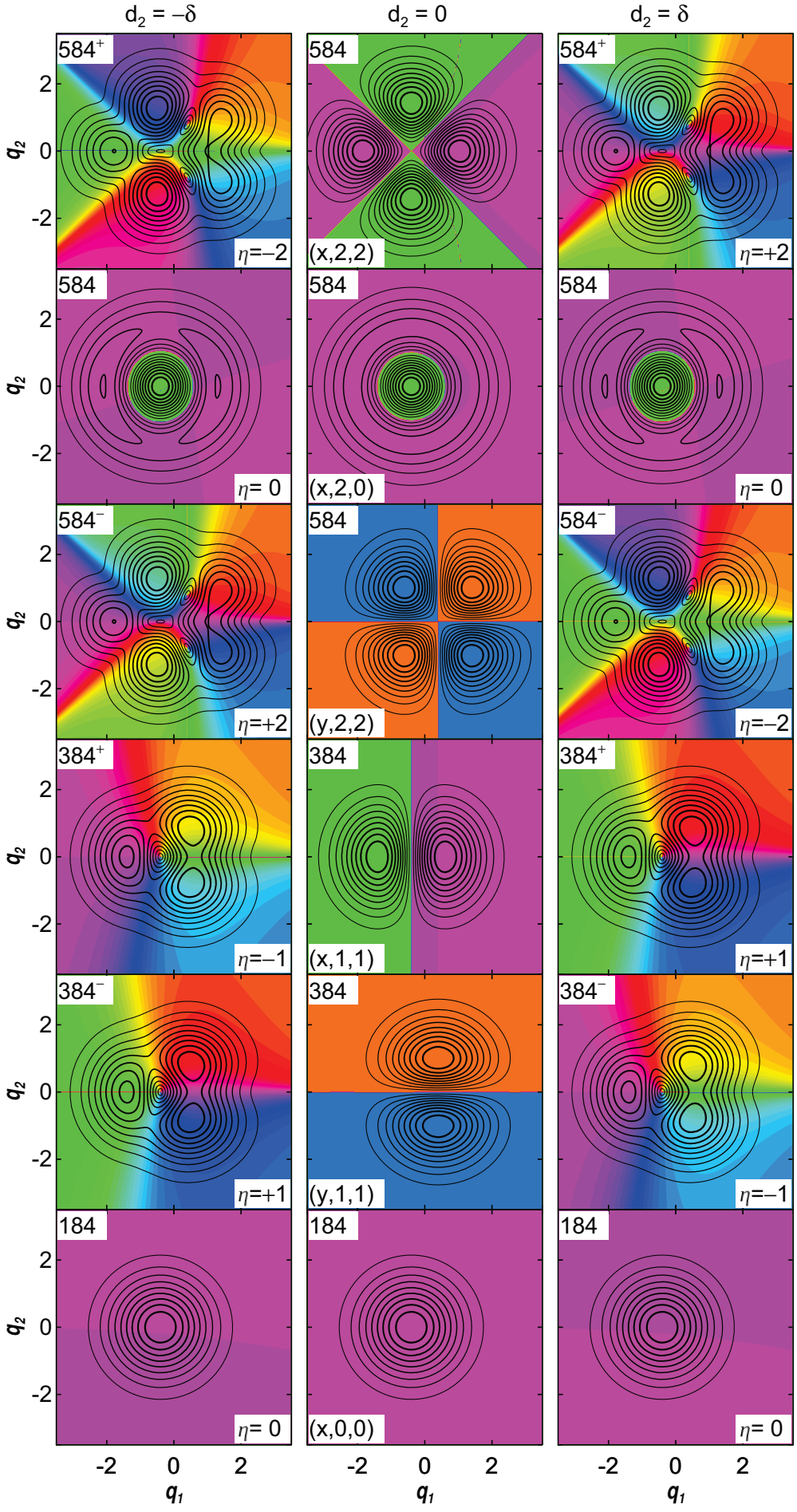
d2 = –δ
d2 = 0
d2 = δ
584+
584
584+
584
584
584
584–
584
584–
384+
384
384+
384–
384
384–
184
184
184
η=–2
(x,2,2)
η=+2
η= 0
(x,2,0)
η= 0
η=+2
(y,2,2)
η=–2
η=–1
(x,1,1)
η=+1
η=+1
(y,1,1)
η=–1
η= 0
(x,0,0)
η= 0
q2
q1
-2
0
2

Figure S4

Figure S4: Nonadiabatic Eigenstates in the Limit of Small but Finite Displacement

The three columns each have six panels showing the probability amplitude and electronic character of the six lowest energy eigenstates with $\sigma_v = +1$ for the Jahn-Teller Hamiltonian with vibrational frequencies $\omega_1 = \omega_2 = 200$ cm^{-1} and Jahn-Teller displacement $d_1 = 0.4$ for the tuning coordinate. The three columns systematically vary the Jahn-Teller displacements d_2 for the coupling coordinate. In each panel, the contour interval is 10% of the maximum probability amplitude for that state, with thicker contour lines for higher amplitude. The color wheel in Figure 1 is used to represent electronic character. In each column, the lowest energy state is on the bottom and energy increases upward. In each panel, the label at upper left gives the eigenstate energy in wavenumbers and the label at lower right specifies the electronic index η for large radius circles. The center column shows an accidental Born-Oppenheimer case with adiabatic nodal lines or curves indicated by abrupt color changes. Degenerate $\sigma_v = +1$ states are chosen so each has a definite adiabatic electronic state (x or y), vibrational quantum number v, and absolute value of the vibrational angular momentum $|l|$ about the equilibrium geometry on its adiabatic potential energy surface given at lower left $(x/y, v, |\ell|)$. The left and right columns show perturbations from the accidental Born-Oppenheimer case with $d_2 = -10^{-10}$ on the left and $d_2 = +10^{-10}$ on the right. Energies of the left and right columns agree with each other to 14-digit precision. The energies with a $+$ or $-$ superscript are slightly above or below the energy for the accidental Born-Oppenheimer case, respectively (see Table S2 and corresponding perturbation theory). The probability amplitudes of the left and right column also agree to 14-digit precision, though the electronic characters differ significantly, with index η reversing with a change in the sign of d_2. Alternately, this can be viewed as showing that η is conserved while the energetic ordering changes as d_2 varies through the degenerate case.

Pertubation theory for two quanta states with small coupling mode displacement

Hougen showed that, when either $d_1 = 0$ or $d_2 = 0$, the Jahn-Teller Hamiltonian accidentally becomes a Born-Oppenheimer Hamiltonian with analytic solutions.[6] When $d_2 = 0$, the diabatic states $|x\rangle$ and $|y\rangle$ become adiabatic electronic eigenstates with different symmetries, so their potential surfaces are allowed to cross. The vibrational coordinates q_1 and q_2 become separable, with harmonic oscillator quantum numbers v_1 and v_2 (this basis is useful even when the vibrational frequencies are different). The harmonic oscillator eigenstates for mode 1 have their equilibria at $q_1|_{eq}^{x} = -d_1$ and $q_1|_{eq}^{y} = +d_1$ on *x* and *y*, respectively, while those for mode 2 both have their equilibria at $q_2|_{eq}^{x} = q_2|_{eq}^{y} = 0$. The degenerate adiabatic states with two vibrational quanta and $\sigma_v = +1$ are:

$$|x20\rangle = |x\rangle|v_1 = 2\rangle|v_2 = 0\rangle,$$

$$|y11\rangle = |y\rangle|v_1 = 1\rangle|v_2 = 1\rangle,$$

and $$|x02\rangle = |x\rangle|v_1 = 0\rangle|v_2 = 2\rangle.$$

Among these three states, two direct couplings arise through the off-diagonal tuning coordinate perturbation operator

$$\hat{H}_1 = \omega_2 \delta \hat{q}_2 [|x\rangle\langle y| + |y\rangle\langle x|].$$

The nonzero direct matrix element couplings are

$$\begin{aligned} H_{\mathrm{x20,y11}} &= \langle v_2^x = 0 | \langle v_1^x = 2 | \langle x | \hat{H}_1 | y \rangle | v_1^y = 1 \rangle | v_2^y = 1 \rangle \\ &= \omega_2 \delta \langle v_1^x = 2 | v_1^y = 1 \rangle \langle v_2^x = 0 | q_2 | v_2^y = 1 \rangle \\ &= \omega_2 \delta \, [2 d_1 (1 - d_1^2) \exp(-d_1^2)][1/\sqrt{2}] \end{aligned}$$

$$\begin{aligned} H_{\mathrm{y11},x02} &= \langle v_2^y = 1 | \langle v_1^y = 1 | \langle y | \hat{H}_1 | x \rangle | v_1^x = 0 \rangle | v_2^x = 2 \rangle \\ &= \omega_2 \delta \langle v_1^y = 1 | v_1^x = 0 \rangle \langle v_2^y = 1 | q_2 | v_2^x = 2 \rangle \\ &= \omega_2 \delta \, [-\sqrt{2} d_1 \exp(-d_1^2)][1] \end{aligned}$$

On the last line of each equation, the first factor in brackets is the Franck-Condon overlap integral for mode 1 (relative to x, the electronic state y is displaced by $+2d_1$), and the second factor in brackets is the harmonic oscillator matrix element for mode 2. For the parameters used in Fig. 3, $H_{y11,x02} \approx$ -9.640906×10^{-9} cm^{-1} and $H_{x20,y11} = -H_{y11,x02}(1-d_1^2) \approx$ 8.098361×10^{-9} cm^{-1}. Degenerate first-order perturbation theory[7] amounts to diagonalizing the truncated 3×3 Hamiltonian matrix coupling the degenerate states:

$$\hat{H}_0 + \hat{H}_1 = \begin{bmatrix} E^{(0)} & H_{x20,y11} & 0 \\ H_{x20,y11} & E^{(0)} & H_{y11,x02} \\ 0 & H_{y11,x02} & E^{(0)} \end{bmatrix}.$$

This yields the eigenvalues

$$E_0^{(1)} = E^{(0)}, \quad E_\pm^{(1)} = E^{(0)} \pm \sqrt{(H_{x20,y11})^2 + (H_{y11,x02})^2}\ .$$

For these three states, all other couplings have effects that are second order in δ. Defining $\Delta = \sqrt{(H_{x20,y11})^2 + (H_{y11,x02})^2}$, this predicts one unshifted state and two states with equal and opposite energetic shifts of $\pm\Delta =$ ±1.259089×10^{-8} cm^{-1}.

The corresponding eigenstates are

$$|\psi_0\rangle = -\frac{H_{y11,x02}}{\Delta}|x\rangle|v_1=2\rangle|v_2=0\rangle + \frac{H_{x20,y11}}{\Delta}|x\rangle|v_1=0\rangle|v_2=2\rangle,$$

$$|\psi_+\rangle = \frac{1}{\sqrt{2}}\left(\frac{H_{x20,y11}}{\Delta}|x\rangle|v_1=2\rangle|v_2=0\rangle + |y\rangle|v_1=1\rangle|v_2=1\rangle + \frac{H_{y11,x02}}{\Delta}|x\rangle|v_1=0\rangle|v_2=2\rangle\right)$$

and $$|\psi_-\rangle = \frac{1}{\sqrt{2}}\left(-\frac{H_{x20,y11}}{\Delta}|x\rangle|v_1=2\rangle|v_2=0\rangle + |y\rangle|v_1=1\rangle|v_2=1\rangle - \frac{H_{y11,x02}}{\Delta}|x\rangle|v_1=0\rangle|v_2=2\rangle\right).$$

The overall signs of these eigenstates were chosen to match the right column of Fig. S4, where δ is positive. The unshifted eigenstate is accidentally adiabatic to first order, so it appears to have a 1D adiabatic nodal curve that becomes a circular node as the displacement of mode 1 tends to zero. In this limit, the unshifted eigenstate becomes the symmetric linear combination state,

$$\begin{aligned}\lim_{d_1\to 0}|\psi_0\rangle &= (1/\sqrt{2})\left(|x\rangle|v_1=2\rangle|v_2=0\rangle + |x\rangle|v_1=0\rangle|v_2=2\rangle\right)\\ &= |x\rangle|v=2,\ell=0\rangle\end{aligned}$$

which is a 2D harmonic oscillator state with zero vibrational angular momentum. Similarly, as $d_1 \to 0$, the shifted eigenstates become symmetric and antisymmetric linear combinations of two real-valued basis states with $\sigma_v = +1$ and an absolute value of 2 for the vibrational angular momentum: the first basis state is the antisymmetric linear combination state on $|x\rangle$,

$$|x\rangle|v=2,|\ell|=2\rangle = (1/\sqrt{2})\left(|x\rangle|v_1=2\rangle|v_2=0\rangle - |x\rangle|v_1=0\rangle|v_2=2\rangle\right);$$

and the second basis state comes from $|y\rangle$,

$$|y\rangle|v=2,|\ell|=2\rangle = |y\rangle|v_1=1\rangle|v_2=1\rangle.$$

For $\delta > 0$, the upper eigenstate is the symmetric linear combination of the above two basis states with $|\ell| = 2$. Since the eigenstates for small d_1 resemble the eigenstates in the limit as $d_1 \to 0$, states with definite absolute values of the angular momentum are plotted in the middle column of Fig. 2 for $\delta = 0$. For finite d_1, the nodal line crossing on $|x\rangle$ is avoided in

$|\psi_{\pm}\rangle$, so that there is nearly a tangential node at $(q_1 = -d_1, q_2 = 0)$. [See the main text results around Fig. 7 and 8 for a description of tangential nodes. Here, a tangential node would occur for the nonadiabatic linear combination states only in the adiabatic limit $d_1 = 0$, where conventional adiabatic nodal lines are a more natural description.] Two conical nodes are approximately located at the crossings between nearly diagonal nodes on $|x\rangle$ and the vertical node at $q_1 = d_1$ on $|y\rangle$. This explains the structure of the *v* = 2 eigenstates in Fig. S4.

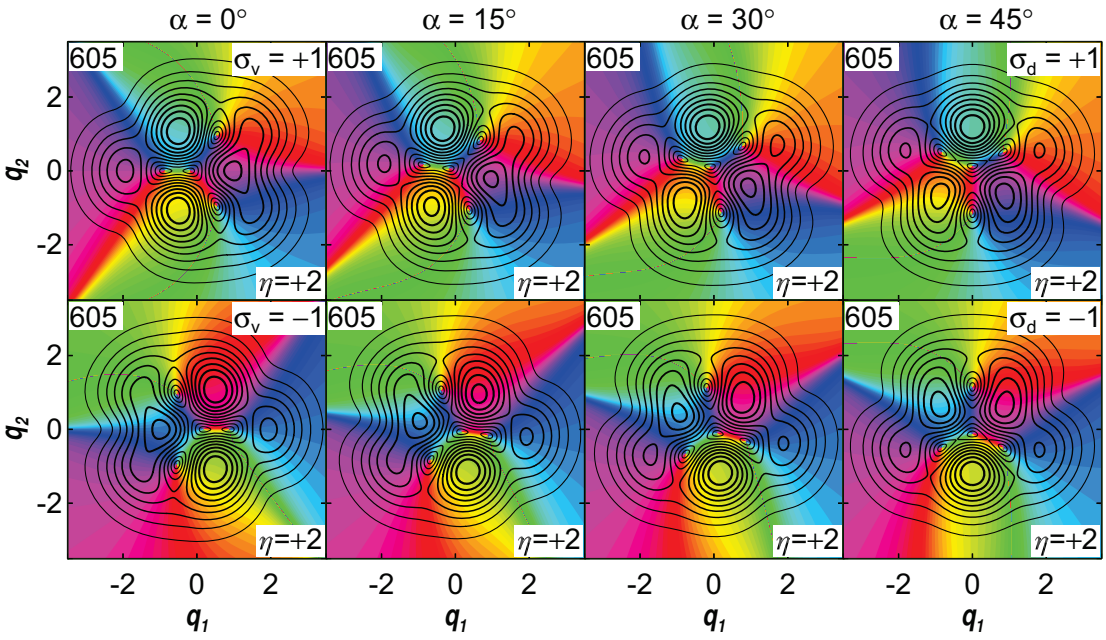

Figure S5

Figure S5: Eigenstates with Different Transformation Angles among Degenerate States

The four panels show how different orthogonal transformations among a degenerate eigenstate pair affect the probability amplitude and electronic character. Each panel shows the 605 cm^{-1} eigenstate of the Jahn-Teller Hamiltonian with vibrational frequencies $\omega_1 = \omega_2 = 200$ cm^{-1} and Jahn-Teller displacements of $d_1 = 0.4$ and $d_2 = 0.2$. The contour interval is 10% and the color wheel from Fig. 1 indicates electronic character. The orthogonal transformation is defined as

$$\begin{bmatrix} |\alpha_+\rangle \\ |\alpha_-\rangle \end{bmatrix} = \begin{bmatrix} \cos(\alpha) & -\sin(\alpha) \\ \sin(\alpha) & \cos(\alpha) \end{bmatrix} \begin{bmatrix} |\sigma_v = +1\rangle \\ |\sigma_v = -1\rangle \end{bmatrix}$$

For $\alpha = \pi/4$, $|\alpha_+\rangle = |\sigma_d = +1\rangle$ and $|\alpha_-\rangle = |\sigma_d = -1\rangle$. The eigenstates in the left panel have σ_v symmetry, while the second panel has the degenerate state pair transformed with $\alpha = 15°$. The third panel has $\alpha = 30°$ and the right panel has $\alpha = 45°$ so that the states exhibit σ_d symmetry. As all nodes are accidental, the location of the nodes is different in each panel, but the electronic index η around the perimeter is conserved.

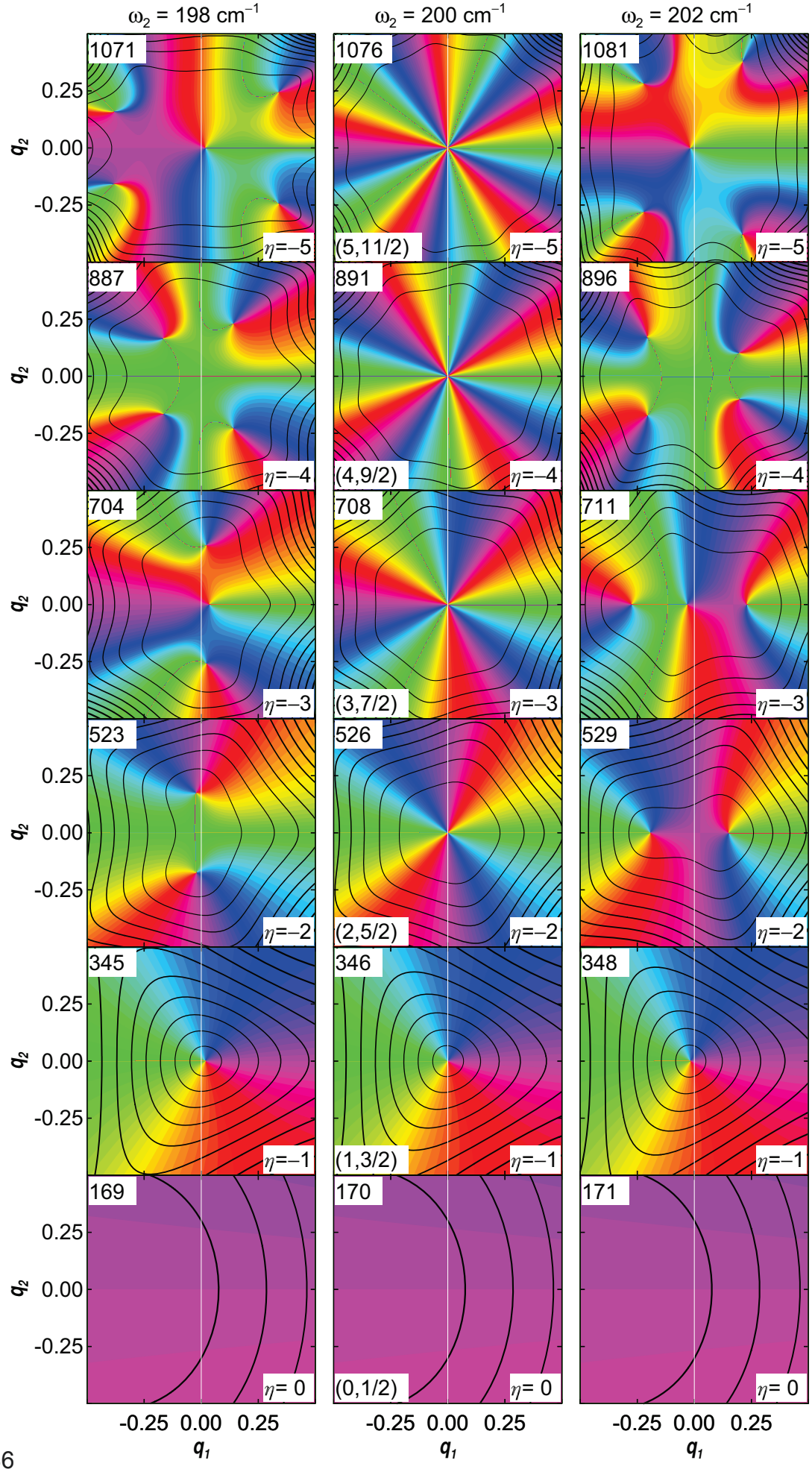
ω2 = 198 cm−1
ω2 = 200 cm−1
ω2 = 202 cm−1
1071
1076
1081
(5,11/2)
η=–5
887
891
896
(4,9/2)
η=–4
704
708
711
(3,7/2)
η=–3
523
526
529
(2,5/2)
η=–2
345
346
348
(1,3/2)
η=–1
169
170
171
(0,1/2)
η= 0
q2
q1
0.25
0.00
-0.25

Figure S6

Figure S6: Splitting of Higher Order Nodes

The probability amplitude and electronic character for six selected eigenstates of the Jahn-Teller Hamiltonian with vibrational frequency $\omega_1 = 200$ cm^{-1} and $d_1 = d_2 = 0.4$. Each column has a different coupling vibration frequency ω_2 given at the top. Energy eigenvalues are given in cm^{-1} at the upper left of each panel. For the bottom two rows, each contour represents 10% of the maximum probability amplitude. For the third row, each contour represents 5% of the maximum probability amplitude, while each contour for the fourth row represents 2% of the maximum probability amplitude, each contour for the fifth row represents 0.5% of the maximum probability amplitude, and each contour for the top (sixth) row represents 0.1% of the maximum probability amplitude. Thicker contours represent higher amplitude. Color represents electronic character as shown in the color wheel in Fig. 1. The eigenfunctions in the center column have circular symmetry and quantum numbers $(v,|j|)$ specified in the lower left of each panel. From bottom to top, they are the lowest energy eigenstate with no node, a first order node, a second order node, a third order node, a fourth order node and a fifth order node, respectively. The columns to the left and right have square-symmetric Jahn-Teller Hamiltonians that generate elliptical conical intersections and have no higher order nodes. In every row, η is conserved for simple closed paths around the perimeter of each panel. A thin white vertical line marking $q_1 = 0$ shows that no node occurs at the origin for the elliptical conical intersections.

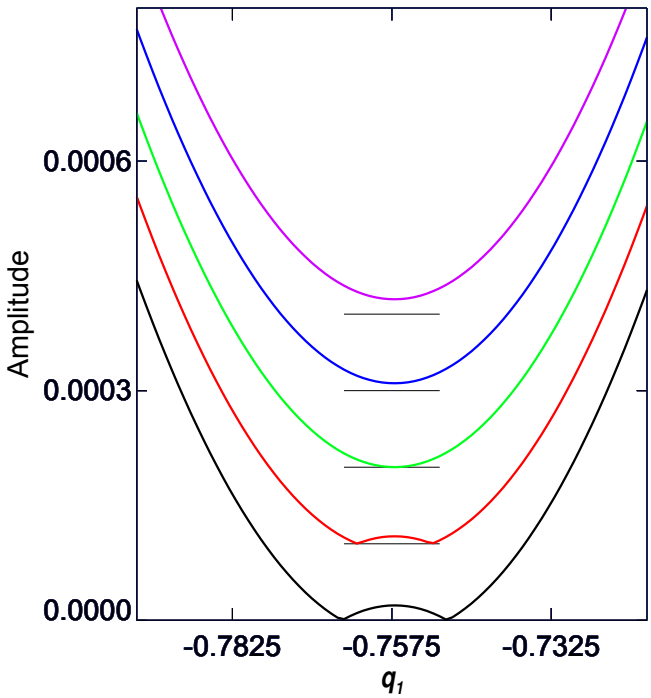

Figure S7

Figure S7: Tangential Node Cross-Sections Through the Tangent Line

Cross-sections along $q_2 = 0$ for the tangential node in Fig. 7 and 8. Relative probability amplitudes as a function of q_1 are offset vertically (by 0.0001) for five different Jahn-Teller Hamiltonians. Each Hamiltonian has a vibrational frequency of $\omega_1 = 200$ cm^{-1} and Jahn-Teller displacements of $d_1 = d_2 = 0.4$; $\omega_2 =$ 230.9005 cm-1 for the black line, 230.903 cm-1 for the red line, 230.90555 cm-1 for the green line, 230.908 cm-1 for the blue line and 230.9105 cm-1 for the violet line. As two conical nodes with opposite signs approach each other, continuity of the total eigenfunction and its derivative along their line of approach requires that the linear term in a Taylor series for the amplitude vanish in between them. This leaves a quadratic term as the lowest order term in the Taylor series expansion of the amplitude along their line of approach.

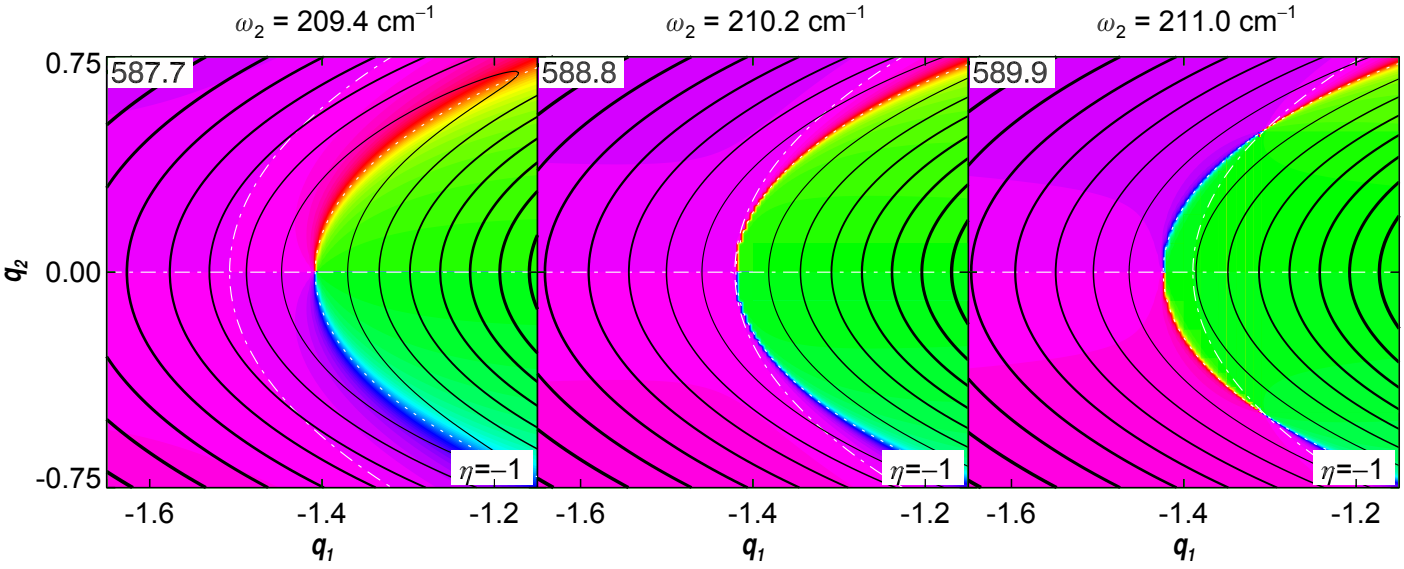
ω_2 = 209.4 cm^{-1}
ω_2 = 210.2 cm^{-1}
ω_2 = 211.0 cm^{-1}
587.7
588.8
589.9
η=–1
η=–1
η=–1
0.75
0.00
-0.75
q_2
-1.6
-1.4
-1.2
q_1

Figure S8

Figure S8: Creation of Three Nodes from a Single First-Order Node

Close up view of the nonadiabatic eigenfunctions correlated to $(v = 2, | j | = 1/2)$ for fixed Jahn-Teller Hamiltonian parameters of $\omega_1 =$ 200 cm^{-1} and $d_1 = d_2 =$ 0.4 as ω_2 (indicated above each panel) increases. The horizontal axis has been stretched by a factor of 3 relative to the vertical axis. The positive vibrational amplitude factor's contour interval is 5%, with thicker contours indicating higher amplitude. The electronic factor is shown using the color wheel from Fig. 1. Each panel overlays the nodal curves in the eigenfunction projections onto adiabatic electronic states *x* (dotted white curve) and *y* (dot-dashed white line). In each panel, the eigenstate energy (cm^{-1}) is given at top left and the total electronic index for a simple closed path around the perimeter is given at lower right. Left) One conical node with electronic index -1 occurs where the nodal curve on *x* intersects the horizontal nodal line on *y*. The nodal curve on *y* lies to the left of the nodal curve on *x* and does not intersect it to generate conical nodes. Middle) At $\omega_2 \approx$ 210.2 cm^{-1}, the vertices of the nodal curves on *x* and *y* coincide with each other at the horizontal nodal line on *y*. Right) The nodal curves on *x* and *y* now cross each other twice (generating two new conical nodes, each with electronic index of -1), and the nodal curve on *x* still crosses the nodal line on *y*, so there are three conical nodes. Compared to the left panel, the node at $q_2 = 0$ has changed its electronic index from -1 to +1. The electronic index for simple closed paths around all these nodes is the sum of the individual electronic indices and remains -1 throughout.

Fig. S8 shows that conical nodes can also be created through a 1 node to 3 node transition as the Hamiltonian parameter ω_2 is increased. Fig. S8 can also be viewed as showing a 3 node to 1 node annihilation event as ω_2 is decreased. In this creation event, nodes are created on top of a previously existing node. This creation involves the intersection of three nodal curves at a single point, a circumstance made possible here by tuning one frequency parameter in the presence of σ_v reflection symmetry. For ω_2 below 210.2 cm^{-1}, the single conical node with $q_2 = 0$ has an electronic index of -1. As ω_2 increases above $210.2\ \mathrm{cm}^{-1}$, two new conical nodes, both with electronic indices of -1, appear above and below the $q_2 = 0$ line. For the same frequency parameter, the electronic index around the node at $q_2 = 0$ changes sign from -1 to +1. The overall index for simple closed paths around this region is the sum of the individual indices and remains -1 throughout. For the value of ω_2 at which nodes are created/annihilated, then, only one node exists and it has an electronic index of -1, so the electronic factor indicates a first order node. As for the shape of the vibrational amplitude around this point, the y character is much less than the x character such that convergence at the 10^{-10} level still shows an amplitude structure closer to that of an adiabatic nodal curve than a tangential node.

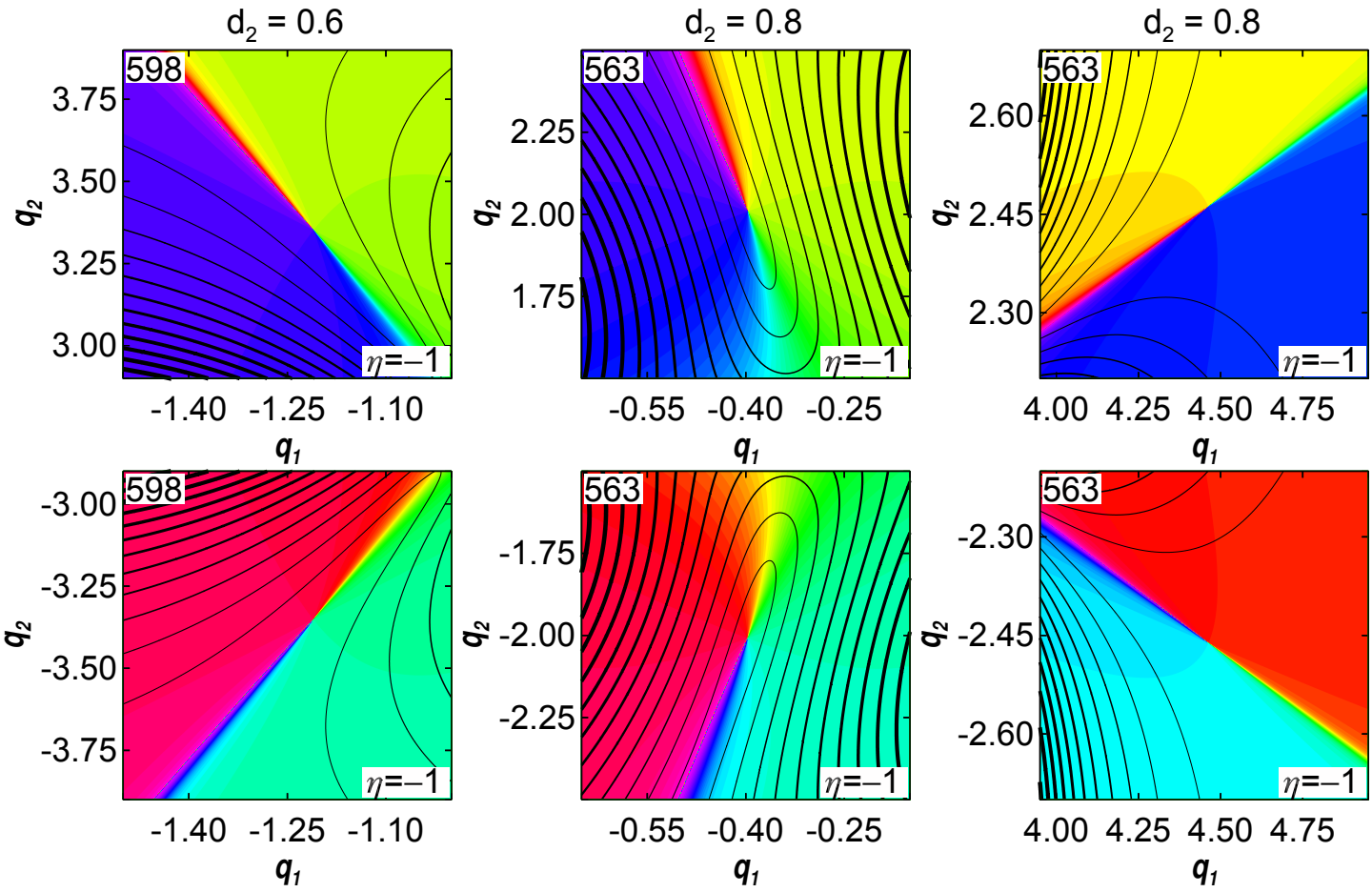
d2 = 0.6
d2 = 0.8
d2 = 0.8
598
563
563
η=–1
q2
q1
3.75
3.50
3.25
3.00
2.25
2.00
1.75
2.60
2.45
2.30
-1.40 -1.25 -1.10
-0.55 -0.40 -0.25
4.00 4.25 4.50 4.75
-3.00
-3.25
-3.50
-3.75
-1.75
-2.00
-2.25
-2.30
-2.45
-2.60

Figure S9

Figure S9: Zoom into Conical Nodes in Figure 9

The six panels show the probability amplitude and electronic character around the conical nodes that are circled in Figure 9. The two panels on the left show close-up views of the sixth lowest energy $\sigma_v = +1$ eigenfunction of the Jahn-Teller Hamiltonian when both vibrational frequencies in the Hamiltonian are $\omega_1 = \omega_2 = 200\ cm^{-1}$, $d_1 = 0.4$ and $d_2 = 0.6$. The contour interval is 0.5%. The four panels in the center and on the right show close-up views of the sixth lowest energy $\sigma_v = +1$ eigenfunction of the Jahn-Teller Hamiltonian when $\omega_1 = \omega_2 = 200\ cm^{-1}$, $d_1 = 0.4$ and $d_2 = 0.8$. The contour interval is 2.5% in the center and 0.025% on the right. All six nodes are shown with uneven aspect ratios to reveal the conical character, which has one highly elongated axis. Due to σ_v symmetry, corresponding nodes in the top row and bottom row have surrounding amplitudes that are reflections of one another and have equal electronic indices.

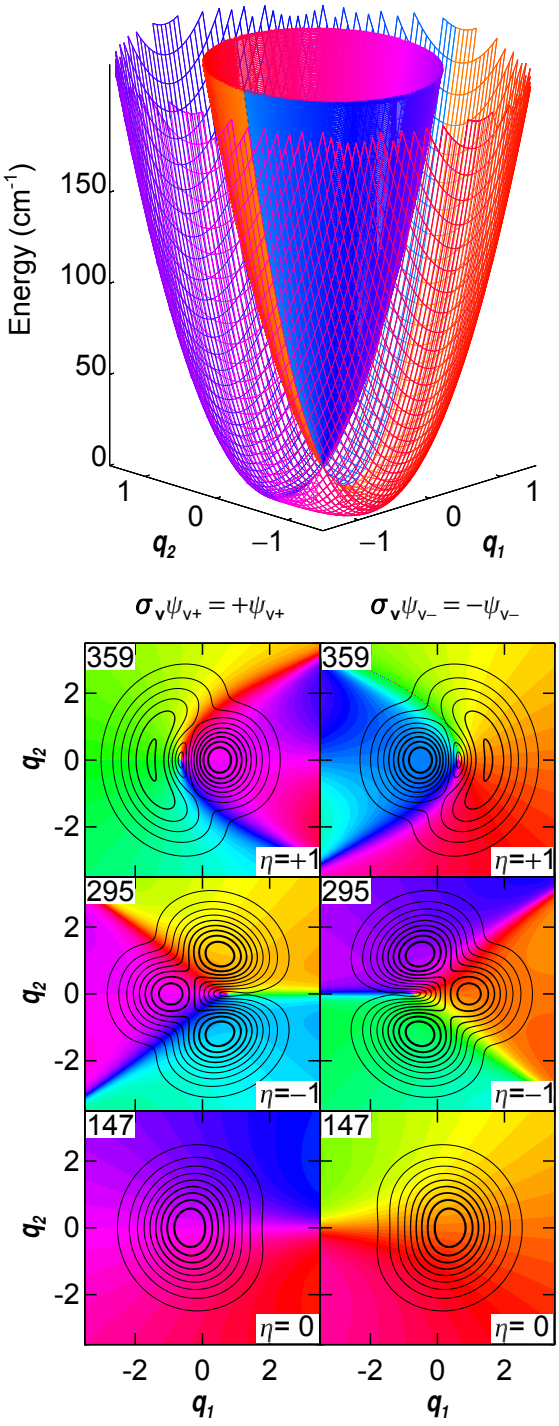
Energy (cm^{-1})
150
100
50
0
1
0
−1
q_2
−1
0
1
q_1
$\sigma_v\psi_{v+} = +\psi_{v+}$
$\sigma_v\psi_{v-} = -\psi_{v-}$
359
359
η=+1
η=+1
295
295
η=−1
η=−1
147
147
η= 0
η= 0
2
0
-2
q_2
-2
0
2
q_1

Figure S10

Figure S10: Adiabatic Potential Surfaces and Nonadiabatic Eigenfunctions for a Conical Intersection with Local Circular Symmetry

Top) The adiabatic potential energy surfaces for a doubly degenerate E symmetry electronic state as a function of Jahn-Teller active normal coordinates (q_1, q_2). The Hamiltonian parameters in Eq. (1) have unequal vibrational frequencies ω_1 =200 cm^{-1} and ω_2 =160 cm^{-1} and unequal displacements d_1 = 0.4 and d_2 = 0.5 such that $\omega_1 d_1 = \omega_2 d_2$. The unequal frequencies make the Hamiltonian and adiabatic potential surfaces globally non-circular, while the last condition gives the conical intersection local circular symmetry. The lower surface has minima [front right and back left] at $(0, \pm d_2)$ that are stabilized $(D\omega)_2$ = 20 cm^{-1} below the conical intersection. The two saddle points [front left and back right] at $(\pm d_1, 0)$ are stabilized by $(D\omega)_1$ = 16 cm^{-1}. The color of each potential surface at each coordinate indicates the adiabatic electronic eigenfunction according to the color wheel in Figure 1. Bottom) The six lowest energy eigenfunctions (shown as eigenstates of σ_v). Contours show probability amplitude, with each contour representing 10% of the maximum amplitude and thicker lines for higher contours. Electronic character is shown by color, again using the color wheel in Figure 1. The asymmetry of these states and the lack of nodes at the conical intersection point (the origin) shows that local circular symmetry is not sufficient to force nodes onto the conical intersection.

146.832358574305
146.832358574306
295.140369817599
295.140369817600
359.209017149936
359.209017149937
449.384364655300
449.384364655301
505.829709426359
505.829709426359
562.967387357872
562.967387357873

Table S3: Energy Eigenvalues for a Conical Intersection with Local Circular Symmetry

Numerical energy eigenvalues (cm^{-1}) for the twelve lowest energy eigenstates of the Jahn-Teller Hamiltonian in Eq. (1) of the main text with the parameters used to generate the adiabatic potential surfaces and nonadiabatic eigenfunctions in Figure S10.

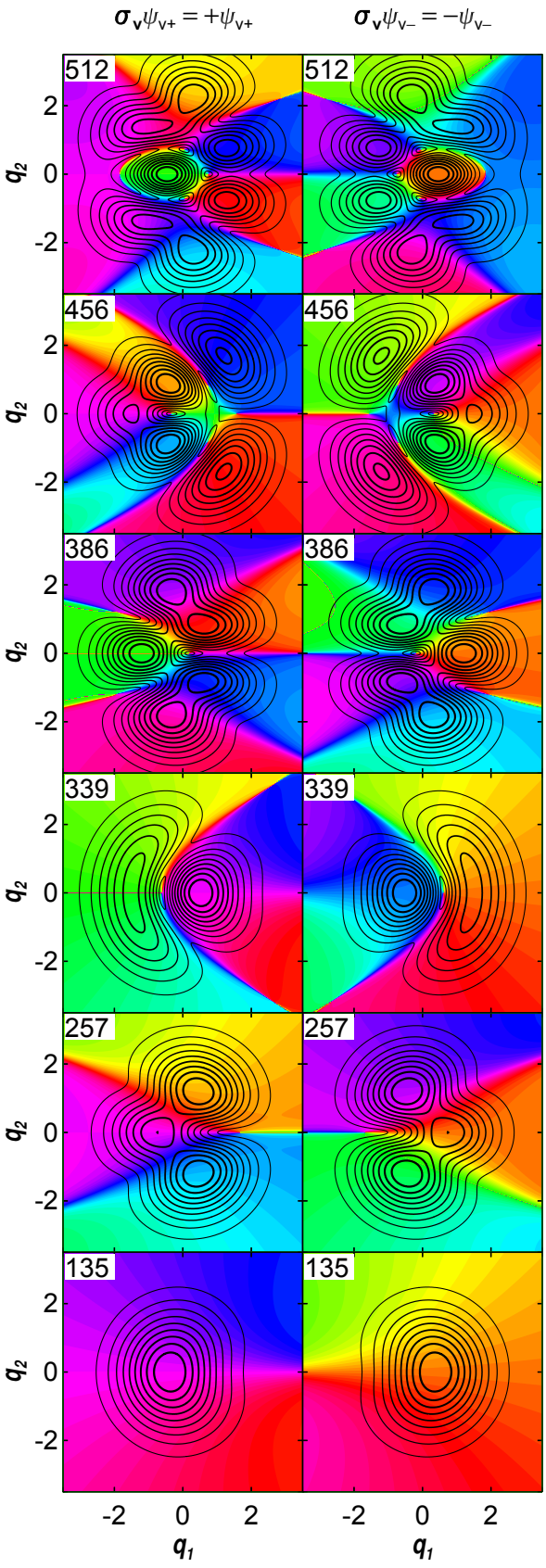
$\sigma_v\psi_{v+} = +\psi_{v+}$
$\sigma_v\psi_{v-} = -\psi_{v-}$
512
512
456
456
386
386
339
339
257
257
135
135
q_2
q_1
-2
0
2

Figure S11

Figure S11: Nonadiabatic Eigenfunctions for a Purely Elliptical Nonadiabatic Hamiltonian

The twelve lowest energy eigenfunctions are shown for a Hamiltonian with unequal vibrational frequencies (ω_1 =200 cm^{-1}, ω_2 =128 cm^{-1}) and unequal Jahn-Teller displacements (d_1 =0.4, d_2 =0.5) chosen to generate the same Jahn-Teller stabilization energy [$(D\omega)$ = 16 cm^{-1}] for both vibrations. All contours of both adiabatic potential energy surfaces are concentric ellipses with exactly the same eccentricity, $e = \sqrt{1-(\omega_2/\omega_1)} = 0.6$. The kinetic energy operator has the same eccentricity, so these eigenfunctions arise from a purely elliptical nonadiabatic Hamiltonian.

134.500041759584
134.500041759585
256.713166795670
256.713166795673
338.978806048831
338.978806048833
385.600744578583
385.600744578585
456.410107135765
456.410107135766
511.741881836435
511.741881836437

Table S4: Energy Eigenvalues for a Purely Elliptical Nonadiabatic Hamiltonian

Numerical energy eigenvalues (cm^{-1}) for the twelve lowest energy eigenstates of Jahn-Teller Hamiltonian in Eq. (1) of the main text with the parameters used to generate the nonadiabatic eigenfunctions in Figure S11.

References for Supplementary Material

[1] H.C. Longuet-Higgins, U. Öpik, M.H.L. Pryce, R.A. Sack, Studies of the Jahn-Teller effect II. The dynamical problem, Proc. R. Soc. Lond. A 244 (1958) 1-16.

[2] P.W. Foster, D.M. Jonas, Nonadiabatic Eigenfunctions Can Have Amplitude, Signed Conical Nodes, or Signed Higher Order Nodes at a Conical Intersection with Circular Symmetry, J. Phys. Chem. A 121 (2017) 7401-7413.

[3] T.C. Thompson, D.G. Truhlar, C.A. Mead, On the form of the adiabatic and diabatic representation and the validity of the adiabatic approximation for X_3 Jahn–Teller systems, J. Chem. Phys. 82 (1985) 2392-2407.

[4] W. Thorson, W. Moffitt, Some Calculations on the Jahn-Teller Effect in Octahedral Systems, Phys. Rev. 168 (1968) 362-369.

[5] B.R. Judd, Exact solutions to a class of Jahn-Teller systems, J. Phys. C: Solid State Phys. 12 (1979) 1685-1692.

[6] J.T. Hougen, Vibronic Interactions in Molecules with a Fourfold Symmetry Axis, J. Mol. Spectrosc. 13 (1964) 149-167.

[7] L.D. Landau, E.M. Lifschitz, Quantum Mechanics, 3rd ed., Pergamon Press, New York, 1977.